Article

Cell Reports

The Interplay between CD27^{dull} and CD27^{bright} B Cells Ensures the Flexibility, Stability, and Resilience of Human B Cell Memory

Graphical Abstract

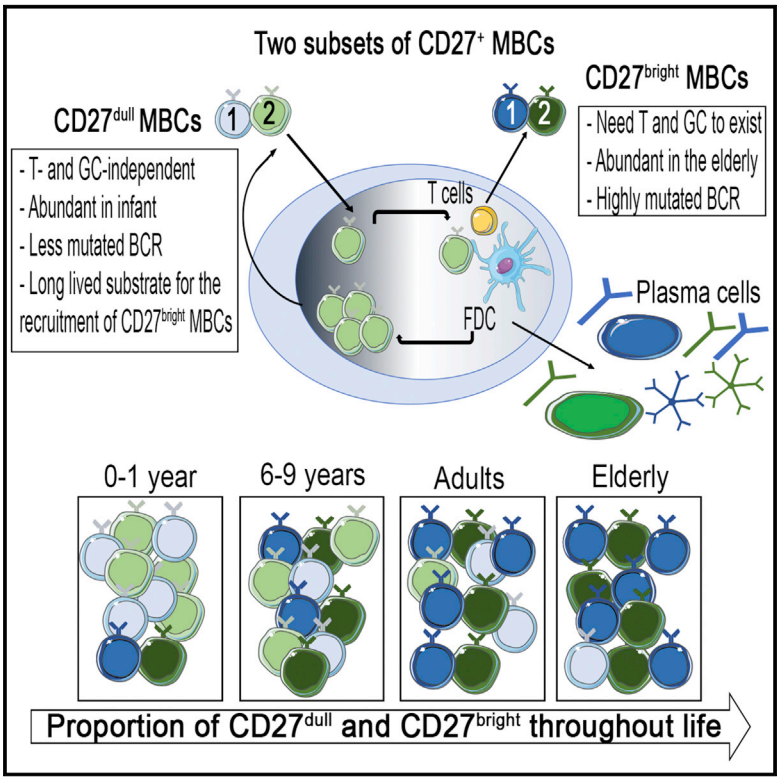

Highlights

- CD27^{dull} and CD27^{bright} MBCs share their VH repertoire but have different functions
- CD27^{dull} MBCs are the long-lived substrate of selected and specific CD27^{bright} MBCs
- The interplay between CD27^{dull} and CD27^{bright} MBCs preserves B cell memory
- In pregnancy, MBCs decline, but persisting CD27^{dull} MBCs re-expand after delivery

Authors

Ola Grimsholm, Eva Piano Mortari, Alexey N. Davydov, ..., Marco Tartaglia, Dmitriy M. Chudakov, Rita Carsetti

Correspondence

rita.carsetti@opbg.net

In Brief

Grimsholm et al. show that CD27^{dull} and CD27^{bright} represent sequential MBC developmental stages. T cell- and germinal center (GC)-independent CD27^{dull} MBCs are the plastic source of strongly selected and GC-dependent CD27^{bright} MBCs. CD27^{dull} MBCs, able to expand and differentiate in response to change, ensure stability and flexibility of human B cell memory.

Grimsholm et al., 2020, Cell Reports *30*, 2963–2977
March 3, 2020
https://doi.org/10.1016/j.celrep.2020.02.022

CellPress

Cell Reports
Article

The Interplay between CD27^{dull} and CD27^{bright} B Cells Ensures the Flexibility, Stability, and Resilience of Human B Cell Memory

Ola Grimsholm,[1,2,22] Eva Piano Mortari,[1,22] Alexey N. Davydov,[3] Mikhail Shugay,[4,5,6] Anna S. Obraztsova,[4,6] Chiara Bocci,[1] Emiliano Marasco,[7] Valentina Marcellini,[1] Alaitz Aranburu,[2] Chiara Farroni,[1] Domenico Alessandro Silvestris,[8] Cristina Cristofoletti,[9] Ezio Giorda,[1] Marco Scarsella,[1] Simona Cascioli,[1] Sabina Barresi,[10] Vassilios Lougaris,[11] Alessandro Plebani,[12] Caterina Cancrini,[12,13] Andrea Finocchi,[12,13] Viviana Moschese,[14] Diletta Valentini,[15] Cristina Vallone,[16] Fabrizio Signore,[16] Giovanni de Vincentiis,[17] Salvatore Zaffina,[18] Giandomenico Russo,[9] Angela Gallo,[8] Franco Locatelli,[8,19] Alberto E. Tozzi,[20] Marco Tartaglia,[10] Dmitriy M. Chudakov,[3,4,5,6] and Rita Carsetti[1,21,23,*]

[1]B Cell Pathophysiology Unit, Immunology Research Area, Bambino Gesù Children's Hospital IRCCS, 00146 Rome, Italy
[2]Department of Rheumatology and Inflammation Research, University of Gothenburg, Box 480, 405 30 Gothenburg, Sweden
[3]Central European Institute of Technology, 625 00 Brno, Czech Republic
[4]Shemyakin and Ovchinnikov Institute of Bioorganic Chemistry, 117997 Moscow, Russia
[5]Institute of Translational Medicine, Pirogov Russian National Research Medical University, 117997 Moscow, Russia
[6]Center of Life Sciences, Skolkovo Institute of Science and Technology, 101000 Moscow, Russia
[7]Division of Rheumatology, Bambino Gesù Children's Hospital IRCCS, 00146 Roma, Italy
[8]Oncohaematology Department, Bambino Gesù Children's Hospital IRCCS, 00146 Rome, Italy
[9]Istituto Dermopatico dell'Immacolata (IDI), IRCCS, 00167 Rome, Italy
[10]Genetics and Rare Diseases Research Division, Bambino Gesù Children's Hospital, 00146 Rome, Italy
[11]Department of Experimental and Clinical Sciences, University of Brescia, 25121 Brescia, Italy
[12]DPUO, Division of Immuno-Infectivology, University Department of Pediatrics, 00146 Bambino Gesù Children's Hospital, Rome, Italy
[13]School of Medicine, University of Tor Vergata, 00133 Rome, Italy
[14]Pediatric Immunology Unit, Policlinico Tor Vergata, University of Rome Tor Vergata, 00133 Rome, Italy
[15]Pediatric and Infectious Disease Unit, Bambino Gesù Children's Hospital, IRCCS, 00146 Rome, Italy
[16]Department of Obstetrics and Gynaecology, Misericordia Hospital Grosseto, Usl Toscana Sud-est, 58100 Grosseto, Italy
[17]Otorhinolaryngology Unit, Bambino Gesù Children's Hospital, IRCSS, 00146 Rome, Italy
[18]Occupational Medicine/Health Technology Assessment and Safety Research Unit, Clinical-Technological Innovations Research Area, Bambino Gesù Children's Hospital, IRCCS, 00146 Rome, Italy
[19]Department of Pediatrics, Sapienza, University of Rome, 00161 Rome, Italy
[20]Multifactorial Disease and Complex Phenotype Research Area, Bambino Gesù Children's Hospital, IRCSS, 00146 Rome, Italy
[21]Diagnostic Immunology Unit, Department of Laboratories, Bambino Gesù Children's Hospital, IRCCS, 00146 Rome, Italy
[22]These authors contributed equally
[23]Lead Contact
*Correspondence: rita.carsetti@opbg.net
https://doi.org/10.1016/j.celrep.2020.02.022

SUMMARY

Memory B cells (MBCs) epitomize the adaptation of the immune system to the environment. We identify two MBC subsets in peripheral blood, CD27^{dull} and CD27^{bright} MBCs, whose frequency changes with age. Heavy chain variable region (VH) usage, somatic mutation frequency replacement-to-silent ratio, and CDR3 property changes, reflecting consecutive selection of highly antigen-specific, low cross-reactive antibody variants, all demonstrate that CD27^{dull} and CD27^{bright} MBCs represent sequential MBC developmental stages, and stringent antigen-driven pressure selects CD27^{dull} into the CD27^{bright} MBC pool. Dynamics of human MBCs are exploited in pregnancy, when 50% of maternal MBCs are lost and CD27^{dull} MBCs transit to the more differentiated CD27^{bright} stage. In the postpartum period, the maternal MBC pool is replenished by the expansion of persistent CD27^{dull} clones. Thus, the stability and flexibility of human B cell memory is ensured by CD27^{dull} MBCs that expand and differentiate in response to change.

INTRODUCTION

The B cell branch of immunological memory, including memory B cells (MBCs), plasma cells (PCs), and their antibodies (Abs), epitomizes the adaptation of the human body to the environment. Immunological memory protects us from re-infection. In the first years of life, children construct their B cell protective system through immune responses to infections and vaccinations, which lead to somatic mutation (SM) of the immunoglobulin (Ig) molecule. In adults, ~50% of the B cells in the peripheral blood (PB) are MBCs (Yoshida et al., 2010).

In the mouse, based on the expression of surface markers, different subsets of MBCs have been identified that are either more naive- or memory-like (Zuccarino-Catania et al., 2014). MBCs of the first subset are poorly mutated and able to form

secondary germinal centers (GCs), whereas those of the second group are highly mutated and immediate precursors of Ab-secreting cells (ASCs) (Zuccarino-Catania et al., 2014). Recently, murine IgM$^+$ MBCs have been demonstrated to function as ''memory'' stem cells able to generate more differentiated MBC effectors (Kenderes et al., 2018).

In humans, most MBCs are CD27$^+$ (Klein et al., 1998). MBCs change in frequency and phenotype with age (Aranburu et al., 2017). Here, we show that, independently of the expressed Ig isotype, MBCs in infants express low levels of CD27 (CD27^{dull}), while in adults, most MBCs are CD27^{bright}. Thus, the description of human MBCs, as either IgM or switched, might be insufficient to encompass the complexity of human B cell memory responses and functions.

During pregnancy, the immune system of the mother suppresses its functions in order to tolerate the fetus (Faas et al., 2014; Parham, 2004; Ruocco et al., 2014; Segerer et al., 2012). In the bone marrow, estrogens inhibit the early stages of B cell development (Yokota et al., 2015) but at the same time increase the proliferation and self-renewal of hematopoietic stem cells (HSCs) (Nakada et al., 2014). In the PB of pregnant women, transitional and MBCs are reduced (Lima et al., 2016).

Here, we examine the two subsets of MBCs, CD27^{dull} and CD27^{bright}, at different ages and conditions over the course of the human lifespan.

We demonstrate that CD27^{dull} MBCs are T cell, GC, and CD40L independent, while CD27^{bright} MBCs are solely generated in individuals with functional GCs. Our combination of transcriptome and immunoglobulin heavy chain (IGH) repertoire analysis and *in vitro* functional assays provides the evidence that CD27^{dull} and CD27^{bright} MBCs represent two sequential MBC developmental stages and that stringent antigen (Ag)-driven pressure selects CD27^{dull} into the CD27^{bright} MBC pool.

We confirm (Schatorjé et al., 2014; Aranburu et al., 2017; Marasco et al., 2017) that the MBC developmental program is implemented in the first 2–3 years of life, starting from CD27^{dull} MBCs. We show that the MBC compartment is altered in the elderly, due to a reduction of CD27^{dull} MBCs. The MBC pool is reshaped in pregnancy when half of the MBCs, mostly CD27^{bright}, are lost. After delivery, CD27^{dull} MBCs increase to reconstitute MBC numbers while preserving the maternal MBC repertoire.

Our results show that in human, highly selected and specific MBCs derive from less refined MBC precursors. We propose that the stability of the human MBC repertoire throughout life is ensured by the existence of CD27^{dull} MBCs that have the capacity to expand and differentiate in response to change. Our model explains the evolution of the B cell response to infectious diseases (Goodwin et al., 2018; Krishnamurty et al., 2016; Pieper et al., 2017; Triller et al., 2017) and provides a rationale for the design of age-tailored vaccination.

RESULTS

Identification, Function, and Ontogeny of CD27^{dull} and CD27^{bright} MBCs

MBCs of infants have low expression of CD27 (CD27^{dull}). At 3–4 years, CD27^{bright} MBCs become detectable. From the age of 6–9 years, CD27^{bright} MBCs increase, reaching the median value of 13% of total B cells in PB. In adults, 23% (median value) of B cells are CD27^{bright} MBCs, and in the elderly, CD27^{bright} MBCs represent 38% of total B cells. CD27^{dull} MBCs, which are the major population in children, are a minority population in adults and rare in older individuals (Figures 1A and 1B). Approximately 60%–80% of the CD27^{dull} MBCs are of IgM type. The proportion of CD27^{dull} MBCs of switched isotypes increases with age (Figure 1C). CD27^{bright} B cells include both IgM and switched MBCs, although most (60%–75%) of them are switched in older individuals (Figure 1D). Extensive phenotyping with a panel of Abs confirmed that several markers discriminate naive from MBCs but none is able to accurately separate CD27^{dull} MBCs from CD27^{bright} MBCs either in adults or in infants (Table S1).

We did not analyze CD27$^-$CD21$^-$ double-negative MBCs, which are rare in normal children and adults. CD27$^-$CD21$^-$ MBCs, also called atypical memory or age-associated B cells, increase with autoimmunity, immunodeficiency, and aging (Colonna-Romano et al., 2009; Moir et al., 2008; Wei et al., 2007; Wu et al., 2011) and include the CD11c^{bright} cells recently described by Wang et al. (2018) (Figure S1).

We previously showed that CD27$^+$ MBCs can be produced by a GC-independent mechanism in the spleen (Aranburu et al., 2017). We now demonstrate that MBCs can be also generated in patients lacking T cells because of primary immunodeficiencies (Table S2), such as T($^-$) natural killer (NK)($^-$) B($^+$) severe combined immunodeficiency (SCID), caused by mutations in *IL2RG* (patients 1 and 2) or *JAK*3 (patient 3) (Fischer, 2000; Roberts et al., 2004). We found that at 6–7 months of life, before receiving curative HSC transplantation, SCID patients had few CD27^{dull} and no CD27^{bright} MBCs (Figure 1E). All MBCs expressed IgM and had a low frequency of SMs (Figure S2; Table S3). Thus, IgM CD27^{dull} MBCs can be generated without T cells.

Patients 4 and 5 (after transplantation) had defects of the common gamma chain (γc). They had received HSC transplantation without pre-conditioning. 10 years after transplantation, T cells were of donor origin, but the patients had maintained their own mutated B cells (Table S2). Signaling through the interleukin-21 (IL-21) receptor, which contains the γc, is indispensable for the completion of the GC reaction (Tangye and Ma, 2020; Zotos et al., 2010). Almost all MBCs of patients 4 and 5 were CD27^{dull} (Figure 1F) and had a low frequency of SMs (Aranburu et al., 2017), suggesting that CD27^{dull} MBCs can be generated even if B cells are unable to maintain and complete the GC reaction. Mutations of the CD40L cause hyper-IgM syndrome type 1. These patients lack GCs, but some MBCs carrying a low number of SMs (Longo et al., 2009; Weller et al., 2001) and expressing IgM could be detected in PB. MBCs of patients with deficiency of CD40L were CD27^{dull} (Figure 1G). Hyper-IgM syndrome type 2 is caused by mutations of activation-induced cytidine deaminase (AID). Patients 9 and 10 had mutations in the N-terminal sequence of AID associated with lack of SM and class-switch recombination (CSR) and the presence of giant GCs (Quartier et al., 2004; Revy et al., 2000). In these cases, both CD27^{dull} and CD27^{bright} MBCs were present at normal frequency in the PB (Figure 1H). These results indicate that the GCs are indispensable for the development of CD27^{bright} MBCs, while AID and SM are instead not required.

As CD27^{bright} MBCs cannot be found in patients unable to generate or carry on the GC reaction, we asked whether

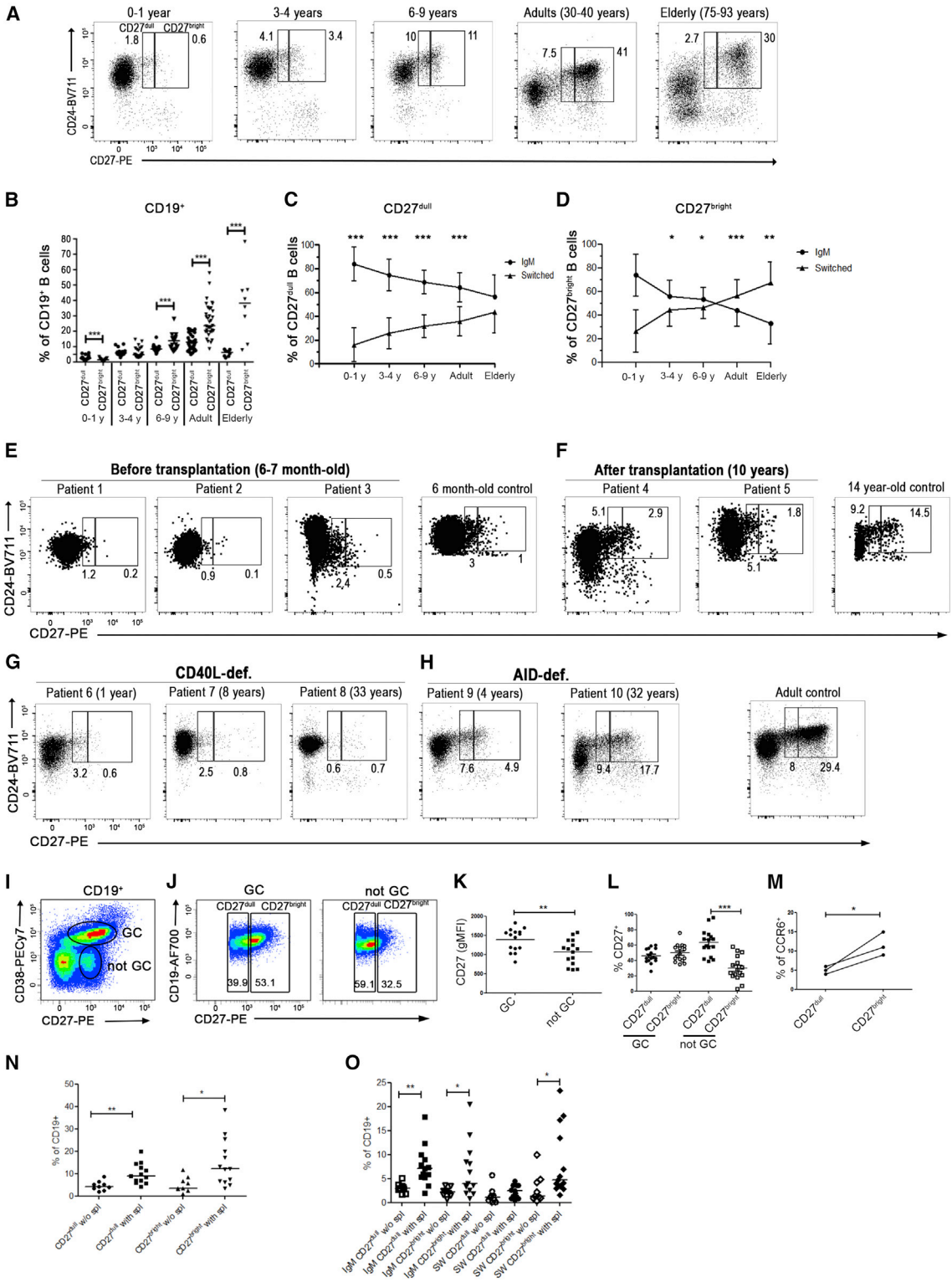

Figure 1. The Two Subsets of the Human CD27^{+} MBC Compartment

(A–D) Flow cytometric analysis of PBMCs from donors of different ages (0–1 year, n = 21; 3–4 years, n = 20; 6–9 years, n = 22; adults 30–40 years, n = 35; elderly 75–93 years, n = 8).

(A and B) Identification (A) and proportion (B) of CD27^{dull} and CD27^{bright} MBCs at the indicated ages. Midlines indicate the median values.

(C and D) Mean of cells expressing IgM or switched isotypes in the CD27^{dull} (C) and CD27^{bright} subsets (D). Errors bars show ± SD.

(legend continued on next page)

CD27^{bright} B cells could be found in the GC of the tonsil. We stained single-cell suspensions from 15 tonsils removed from children between 2.7 and 6.3 years of age (Figure 1I). We compared the intensity of staining (gMFI) for CD27 in GC B cells (CD3$^-$CD19$^+$CD38$^+$) and non-GC MBCs (CD3$^-$CD19$^+$CD38$^-$) in each sample (Figure 1J). GC B cells expressed significantly more CD27 than non-GC MBCs (Figure 1K). In children, in tonsil as in PB, most MBCs included in the non-GC gate were CD27^{dull}, while in the GC gate, CD27^{dull} and CD27^{bright} B cells were found at comparable frequencies (Figure 1L). CCR6 has been recently identified as a marker able to distinguish MBC precursors in the GC (Suan et al., 2017). We found CCR6$^+$ B cells to be enriched in the CD27^{bright} GC population (Figure 1M). In the non-GC population, as previously reported (Suan et al., 2017), 95% of MBCs express CCR6$^+$, and we did not see any difference between CD27^{dull} and CD27^{bright} (data not shown).

We have demonstrated before that in asplenic and splenectomized patients, IgM MBCs are strongly reduced (Kruetzmann et al., 2003; Piano Mortari et al., 2017), whereas switched MBC numbers are in the normal range. Ivemark syndrome (IS), a complex malformation of the heart, can be associated with asplenia (Piano Mortari et al., 2017). We compared the frequency of CD27^{dull} and CD27^{bright} MBCs in nine patients with IS born without a spleen and 13 IS patients with a normal spleen. We found that both CD27^{dull} and CD27^{bright} MBCs were significantly reduced in the absence of a spleen (Figures 1N and S3A). This result is explained by the loss of IgM MBCs in the CD27^{dull} and CD27^{bright} populations (Figures 1O and S3B). In contrast, MBCs expressing switched isotypes were significantly reduced only in the CD27^{bright} MBCs (Figures 1O and S3B).

Separate Functions of CD27^{dull} and CD27^{bright} MBCs *In Vitro*

Human MBCs proliferate and differentiate into PCs by stimulation with the Toll-like receptor 9 (TLR9) agonist CpG (Bernasconi et al., 2003; Capolunghi et al., 2008). CD27^{dull} and CD27^{bright} MBCs were sorted (the sorting strategy is described in Figure S3C), loaded with carboxyfluorescein succinimidyl ester (CFSE), and stimulated with CpG (Marasco et al., 2017). Sorted naive B cells were used for comparison. After 5 days of stimulation, CD27^{bright} MBCs had proliferated significantly more than CD27^{dull} MBCs (proliferation index; Figures 2A and 2B) and produced more plasmablasts (PBLs) (Figure 2C). IgM was expressed on the surface of 60% of the PBLs generated from the CD27^{dull} population, whereas most of the PBLs derived from CD27^{bright} MBCs were IgM$^-$ (Figure 2D) and expressed either IgG (two-thirds of the IgM$^-$) or IgA (one-third of the IgM$^-$) intracellularly. The expression of the PC master regulator *Prdm1* was higher in CD27^{bright} MBCs than in CD27^{dull} MBCs (Figure 2E). By ELISpot, we confirmed that CD27^{bright} MBCs generated mostly IgA- and IgG-secreting cells (Figure 2F). IgM Ag-specific ASCs can be generated from both CD27^{dull} and CD27^{bright} MBCs, whereas IgG and IgA ASCs specific for tetanus toxoid and pneumococcal polysaccharides belong to the CD27^{bright} MBC population (Figure 2F). CD40L, in combination with anti-Ig and IL-21, is used as prototypical T-dependent stimulus *in vitro* (Marasco et al., 2017). More naive B cells divide in response to CD40L, compared to the two MBC populations (Figure 2G), but do not differentiate into PBLs. CD27^{bright} MBCs were more effective in generating PBLs than CD27^{dull} MBCs (Figure 2H). Expression of *AICDA*, encoding for the crucial enzyme for SM and CSR, was induced in both CD27^{dull} and CD27^{bright} MBCs at a higher level than in naive B cells (Figure 2I). Thus, in comparison to naive B cells, CD27^{dull} and CD27^{bright} MBCs respond better to CpG and show an increased ability to upregulate *AICDA* in response to CD40L. CD27^{bright} MBCs are more able to generate ASCs in comparison to CD27^{dull} MBCs.

Transcriptional Profiling of Human CD27^{dull} and CD27^{bright} MBCs

In order to define CD27^{dull} and CD27^{bright} MBCs by their function, we compared their gene expression profiles as generated by RNA sequencing (RNA-seq). Using naive B cells as controls, we sorted the two MBC populations from four different healthy donors (HDs) aged 28–48 years (sorting gates are shown in Figure S3C). We obtained ~30 million reads from each sample and compared the transcriptomes of the three sorted populations by principal-component analysis (unsupervised) (Figure 3A). The first principal component (PC1) separates CD27^{bright}, CD27^{dull}, and naive B cells into three distinct clusters, indicating that, from a transcriptional point of view, naive B cells are very different from both types of MBCs. CD27^{dull} and CD27^{bright} MBCs are also different from each other. The second principal component (PC2) separates the samples according to donor

(B–D) Statistical significances were determined using unpaired, two-tailed Mann-Whitney *U* tests (*p ≤ 0.05, **p < 0.01, and ***p < 0.001).
(E–H) Flow cytometric staining of PBMCs from controls and patients with T$^-$NK$^-$B$^+$ SCID before (n = 3) (E) and after HSC transplantation (n = 2) (F), and patients with CD40L deficiency (n = 3) (G) and AID deficiency (n = 2) (H). Plots show the frequency of CD19$^+$ B cells that are either CD27^{dull} or CD27^{bright} MBCs in the indicated patients.
(I–M) Flow cytometric analysis of tonsil cells stained for CD27 and CD38 to identify B cells belonging to the GC or not (representative of 15 experiments).
(I) Gating used to identify GC or non-GC populations.
(J) Identification of CD27^{dull} and CD27^{bright} MBCs within GC and non-GC populations.
(K) gMFI for CD27 in GC and non-GC cells.
(L) Percentage of CD27^{dull} and CD27^{bright} MBCs in GC and non-GC populations.
(M) Frequency of CCR6$^+$ B cells in CD27^{dull} and CD27^{bright} MBCs of the GC.
(K and L) Midlines indicate mean values.
(K–M) Statistical significance was determined using unpaired, two-tailed Student's t tests (*p ≤ 0.05, **p < 0.01, and ***p < 0.001).
(N) Graph shows the frequency of CD27^{dull} and CD27^{bright} MBCs in PBMCs of IS patients born with (n = 13) or without spleen (spl) (n = 9). Midlines indicate median. Statistical significance was determined using an unpaired, two-tailed Student's t test (*p < 0.05 and **p < 0.01).
(O) Frequency of CD27^{dull} and CD27^{bright} MBCs expressing either IgM or switched (SW) isotypes in IS patients with and without spleen. Midlines indicate the median values. Statistical significance was determined using unpaired, two-tailed Mann-Whitney *U* tests (*p ≤ 0.05 and **p < 0.01).

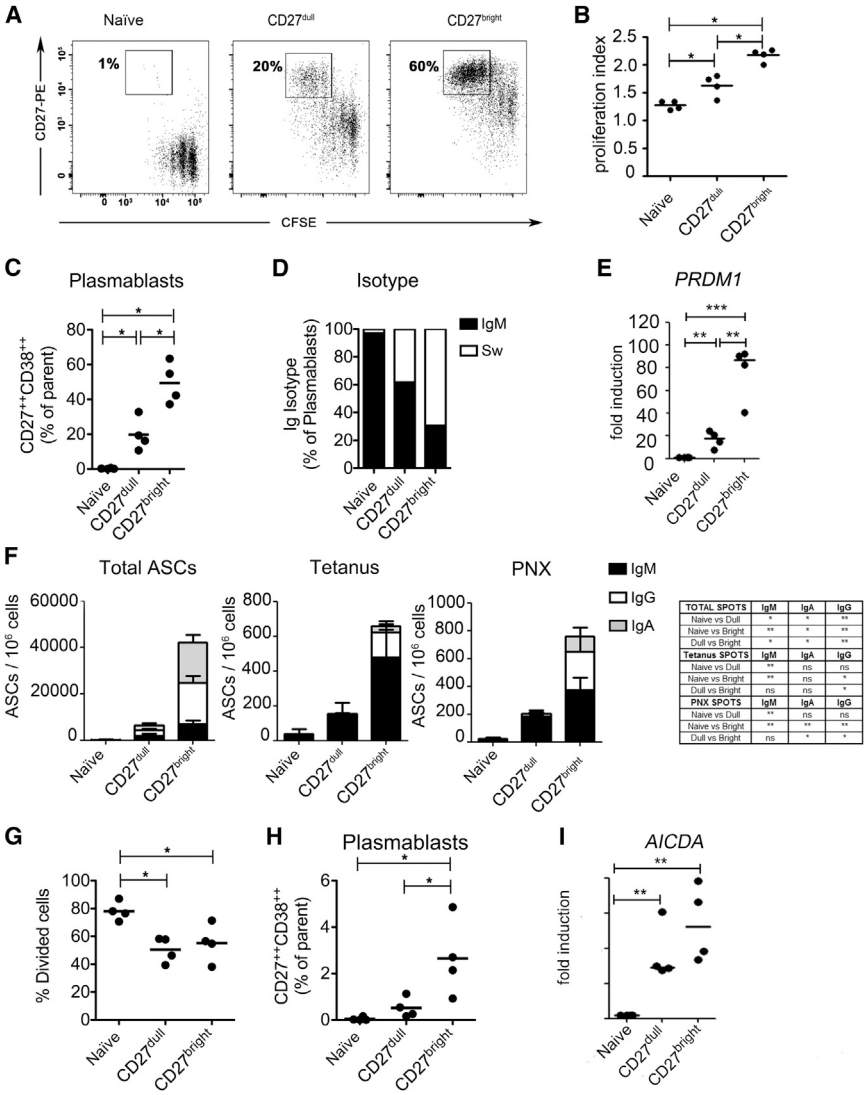

Figure 2. Functional Differences in CD27^{dull} and CD27^{bright} MBCs

(A–F) Naive, CD27^{dull}, and CD27^{bright} MBCs from adult HDs (age range, 30–40 years) were sorted and stimulated with CpG for 5 days.

(A) PBLs are identified as CD27^{+++} CFSE^{low} cells. FACS plots are representative of four independent experiments. CD27^{+++}CFSE^{low} are also CD38^{++}.

(B and C) Proliferation index (B) and percentage of PBLs (CD27^{++}CD38^{++}) in the indicated cultures (C).

(D) Ig isotype as percentage of the PBLs.

(E) *Prdm1* mRNA expression (normalized to ACTB) in naive, CD27^{dull}, and CD27^{bright} MBCs. Statistical significance was determined by unpaired, two-tailed Student's t tests (**p < 0.01 and ***p < 0.001). Midlines indicate median.

(F) Total (left panel), tetanus-specific (middle panel), and pneumococcal polysaccharides (PNX)-specific (right panel) ASCs measured by ELISpot. The proportions of IgM, IgG, and IgA isotypes for each population are depicted by bars. The table indicates statistical significance determined by unpaired, two-tailed Mann-Whitney *U* tests (*p ≤ 0.05 and **p < 0.01). Errors bars show ± SD.

(G–I) Naive, CD27^{dull}, and CD27^{bright} MBCs were sorted and stimulated with CD40L + anti-Ig + IL-21 for 5 days.

(G and H) Graphs show the percentage of (G) divided cells and the percentage of (H) PBLs (CD27^{+++}CD38^{++}) in the indicated cultures.

(I) mRNA expression of *Aicda* after 5 days of stimulation in the indicated cultures (normalized to ACTB). Statistical significance was determined by unpaired, two-tailed Student's t tests (**p < 0.01). Midlines indicate median.

(A–I) All experimental data were obtained from four separate experiments with sorted cells from different adult HDs (n = 4). (B, C, G, and H) Midlines show medians. Statistical significance was calculated using unpaired, two-tailed Mann-Whitney *U* tests (*p ≤ 0.05).

origin. Given the variability of the genetic background among individuals, the clear separation of naive, CD27^{dull}, and CD27^{bright} MBCs into three clusters supports our hypothesis that the three populations represent separate pools. The Venn diagrams (Figure 3B; Table S4) show the number of genes that are significantly ($p \leq 0.05$) up- or downregulated in the comparison among naive, CD27^{dull}, and CD27^{bright} MBCs, confirming that the transcriptome of MBCs, both CD27^{dull} and CD27^{bright}, is different from that of naive B cells and also that the two MBC populations are different from each other (Figure 3B).

We confirmed by qPCR and flow cytometry the results obtained by RNA-seq in independent sets of adult and children donors. We sorted CD27^{dull} and CD27^{bright} MBCs from PB of adults and 1- to 3-year-old children. By qPCR, we verified six genes highlighted as significantly different (three upregulated and three downregulated in MBCs) by RNA-seq analysis (Figure S4A; Tables S5–S7). Abs against proteins encoded by five genes identified by the RNA-seq analysis were used for confirmation by flow cytometry in adults (Figure S4B) and children (Figure S4C). The results confirm the RNA-seq findings. The comparable expression of the studied genes in infants and adults suggests that the gene expression pattern of CD27^{dull} and CD27^{bright} MBCs is similar at different ages.

In Figure 3, the heatmaps show the top 50 genes differentially expressed by naive B cells and CD27^{dull} MBCs, naive B cells and CD27^{bright} MBCs, and finally CD27^{dull} and CD27^{bright} MBCs (Figure 3C).

We focused on genes that play a role during the peripheral differentiation pathway initiating from transitional or naive B cells and leading to MBCs and PCs. The comparison identifies a signature that is established in CD27^{dull} MBCs and strengthened in CD27^{bright} MBCs (Figures 3D and S5). When we compared directly the two types of MBCs, we found that based on the expression of all signature genes, CD27^{dull} MBCs are more "naive-like," whereas CD27^{bright} MBCs are more "memory-like" (Figure 3D).

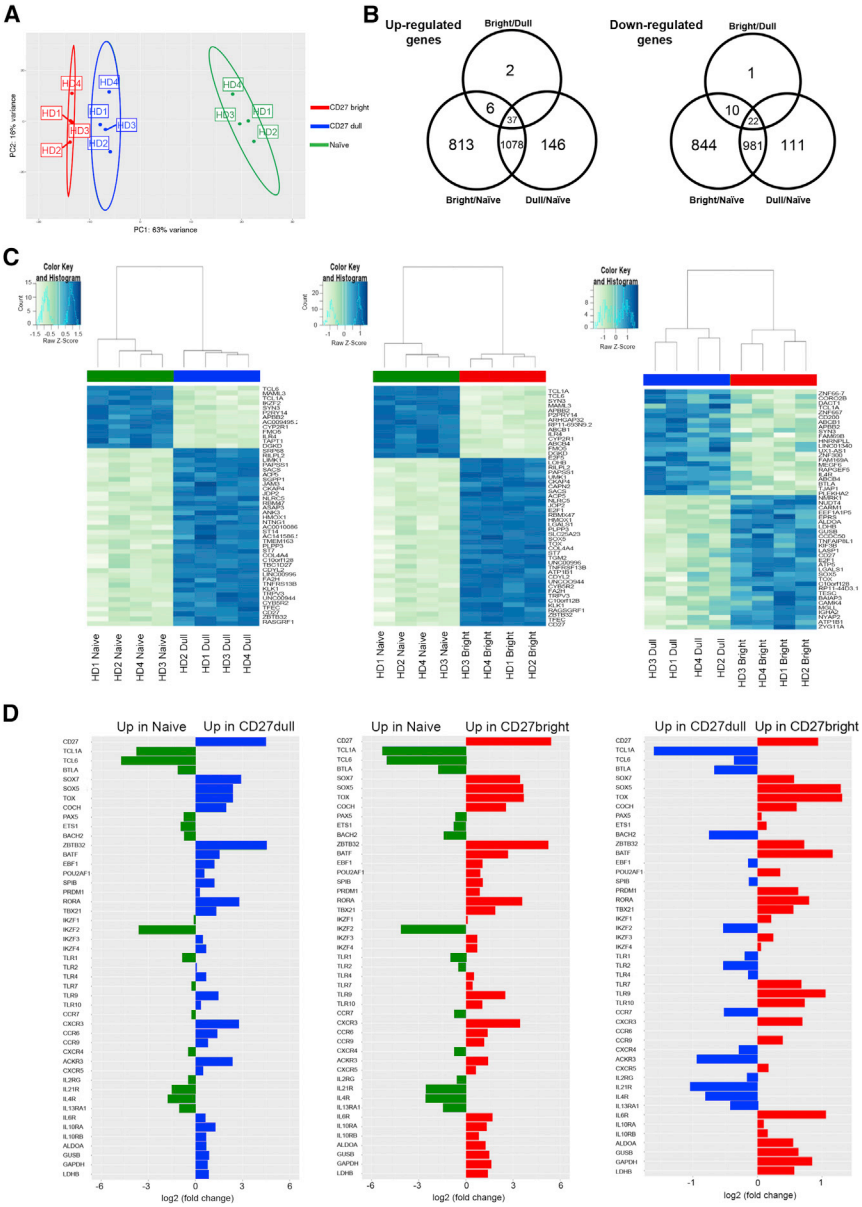

Figure 3. Gene Expression Profile of Sorted Naive, CD27^{dull}, and CD27^{bright} MBCs

(A) Gene expression based principal-component analysis (PCA). Axes represent the first two principal components, labeled with the percentage of total variance explained by each. Each dot represents one of the 12 samples (four biological replicates for each condition), with colors indicating the different populations of B cells. The first two principal components account for ~80% of the variance in the population of the compared samples.

(B) Venn diagram showing overlaps and differences between genes that were significantly ($p \leq 0.05$) upregulated (left panel) and downregulated (right panel) in naive, CD27^{dull}, and CD27^{bright} MBCs.

(C) Heatmaps of the top 50 differentially expressed genes comparing naive versus CD27^{dull} (left panel), naive versus CD27^{bright} (middle panel), and CD27^{dull} versus CD27^{bright} (right panel). Data were clustered based on the expression levels of the selected top 50 genes. Up- or downregulation levels are reported as *Z* scores (representing the deviation from the mean by standard deviation units) scaled by row.

(D) Barplots showing relative expression levels, reported as log2 (fold change), for genes encoding B cell transcription factors, Ikaros family, Toll-like receptors, chemokine receptors, and cytokine receptors in naive, CD27^{dull}, and CD27^{bright} MBCs. Data in (B) and (C) are from one experiment with cells sorted from four HDs.

Shared VH Repertoire and Different Frequency of SM in CD27^{dull} and CD27^{bright} MBCs

In order to compare the VH repertoires of naive B cells, CD27^{dull} MBCs, and CD27^{bright} MBCs, we sorted the three different B cell populations from PB samples of four HDs aged 37–57 years. We employed a cDNA-based 5′ rapid amplification of cDNA ends (RACE) approach with unique molecular identifiers (Turchaninova et al., 2016) in order to generate full-length Ig sequences that are nearly error-free.

Bioinformatic analysis of B cell repertoires revealed a number of Ig sequence features that differ among the three subsets and are related to the structure of VDJ rearrangements, physicochemical characteristics of the CDR3 region, clonotype sharing, and the process of affinity maturation.

Remarkably, immunoglobulin heavy chain variable (IGHV) gene segment usage frequency was generally similar within VH repertoires of naive B cells of different donors, which, for this reason, clustered together (Figure 4A). This observation is in line with the finding that the frequency of selection of different IGHV gene segments in the naive Ig repertoire is generally similar across Caucasians (Watson et al., 2017). The VH repertoire of MBCs was different from that of naive B cells, as expected, since MBC Ig genes are selected and shaped by the immune response.

IGHV gene segment usage was similar between the CD27^{dull} and CD27^{bright} MBCs of the same donor but different between the four subjects included in our study (Figure 4A), suggesting that the two MBC subsets share a notable portion of memory clones generated by the individual antigenic experience.

To verify the latter hypothesis, we analyzed the intra-individual overlaps of clonally shared CDR3 variants between normalized CD27^{dull} and CD27^{bright} MBCs, CD27^{dull} MBCs and naive B cells, CD27^{bright} MBCs, and naive B cell repertoires. As expected, overlap within naive B cell repertoires was negligible. CD27^{dull} and CD27^{bright} MBCs, on the other hand, overlapped substantially (Figure 4B). To give some intuitively clear estimation, 20–165 (average, 85) CDR3 variants were shared between the top

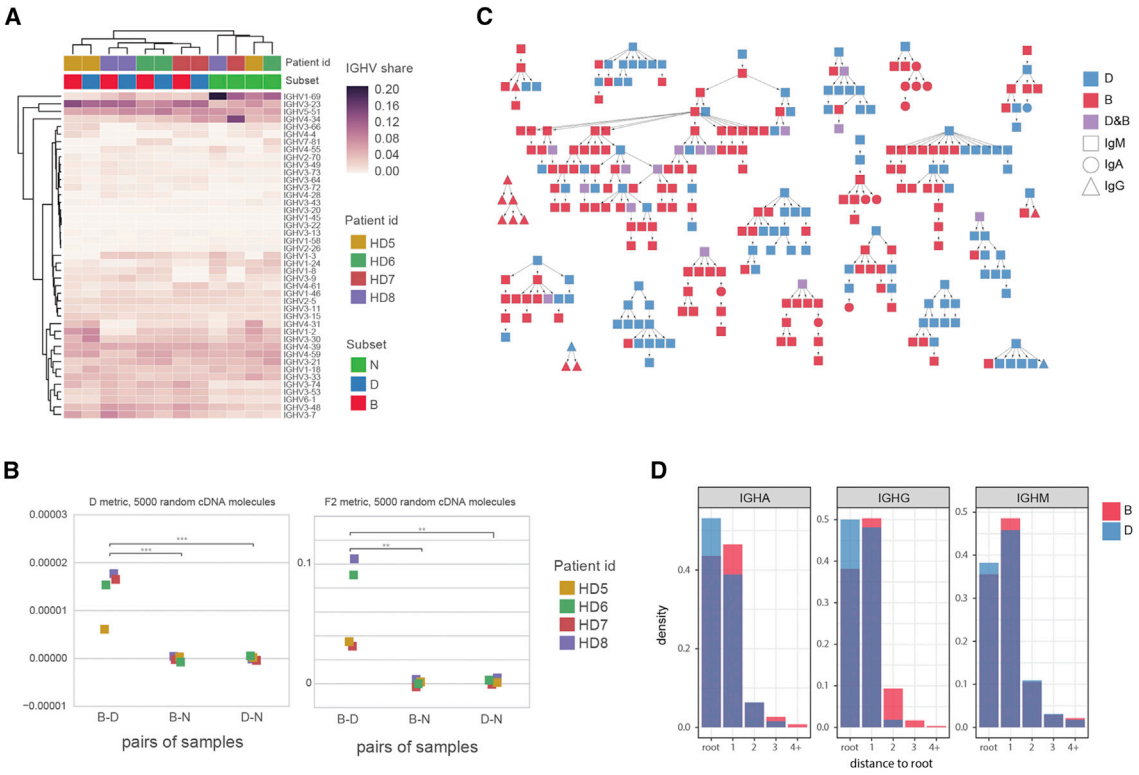

Figure 4. Basic Characteristics of Ig Repertoires

(A) IGHV gene segments usage, weighted (per cDNA molecule), showing co-clustering of naive B cell repertoires of different donors and co-clustering of CD27^{dull} and CD27^{bright} MBCs of the same individuals.

(B) Overlap of Ig repertoires measured for the normalized samples (5,000 randomly selected Ig cDNA molecules per sample) using unweighted (D, reflects the number of shared unique clonotype sequences) and weighted (F2, reflects the number of cDNA molecules sharing particular sequences); metrics were computed using VDJtools software. Significant overlap was observed between the repertoires obtained for CD27^{dull} and CD27^{bright} MBCs. *$p < 0.01$ and **$p < 0.001$.

(C) Hypermutating IGH trees demonstrating the multilayer clonal interspersion of CD27^{dull} and CD27^{bright} subsets. Note that our analysis is limited by sampling depth and thus is not covering the full pre-history of the hypermutation process. Therefore, apparently impossible isotype conversions can be observed within hypermutating trees that could be explained by missing intermediate IGH variants.

(D) The distribution of distances to the root of hypermutated IGH trees for CD27^{dull} and CD27^{bright} clonotypes. CD27^{bright} clonotypes are further away from the ancestor for all isotypes (Mann-Whitney *U* test: IgG, $p = 0.017$; IgA, $p = 0.029$; IgM, $p = 0.024$).

1,000 clonotypes of CD27^{dull} and CD27^{bright} subsets of the same individual. The overlap grows with the depth of repertoire analysis (Kosmrlj et al., 2008), suggesting that a large proportion of clones are shared between the two subsets, and thus, many CD27^{dull} clones could at some point be selected and convert to the CD27^{bright} phenotype.

CD27^{dull} and CD27^{bright} IGH sequence variants were interspersed within hypermutating trees (Figures 4C and S6). By quantifying the distance to the roots of CD27^{dull} and CD27^{bright} IGH variants, we found that, on average, CD27^{dull} IGH variants were distributed closer to the roots of the trees (Figure 4D) (i.e., were identified as less hypermutated sequence variants). These observations indicate that conversion from one population to another happens repeatedly, and populational plasticity represents a multilayer process, with CD27^{dull} MBCs being long-lived and providing substrate for the generation of CD27^{bright} MBCs.

At the same time, in spite of intra-individual similarity of IGHV gene segment usage, notable clonal overlap, and interspersion of hypermutating trees, further analyses demonstrated that CD27^{dull} and CD27^{bright} repertoires are clearly distinct in terms of Ab features and acquired SM.

In particular, analysis of averaged CDR3 repertoire characteristics using VDJtools software revealed that CDR3 length, as well as physico-chemical characteristics of amino acid residues located in the middle of CDR3 differ between the two MBC subsets (Figure 5A). The latter included estimated "energy" of the interaction with pMHC[41], "strength" of the interaction (derivative of "energy," VDJtools), and a number of Kidera factors, such as hydrophobicity (Kidera factor 4). Altogether, the observed changes from naive B cells to CD27^{dull} and to CD27^{bright} subsets consolidate as a trend toward a sequential decrease of CDR3 length and of the number of bulky, hydrophobic, and strongly interacting (Kosmrlj et al., 2008; Miyazawa and Jernigan, 1996) amino acid residues in the middle of the CDR3. These changes could be interpreted as peripheral selection and evolution of VH repertoires leading to the elimination of Ig variants that are nonspecifically too "sticky" and thus cross-reactive (Kosmrlj et al., 2008; Stadinski et al., 2016). Such selection would involve at least two sequential stages, both of which

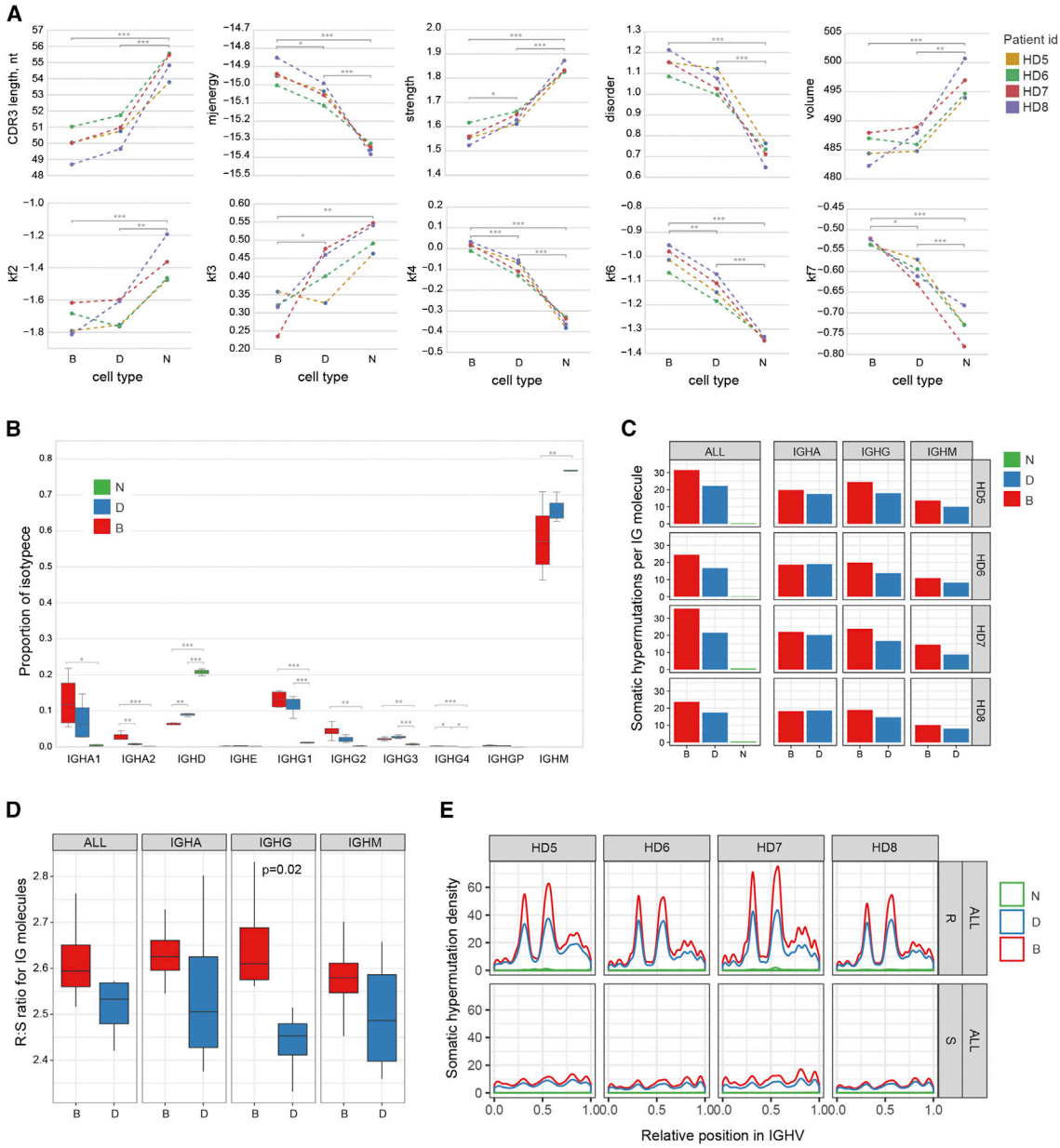

Figure 5. Isotype Switching and Somatic Hypermutation Patterns

(A) Weighted (per cDNA molecule; i.e., accounting for clonal size) characteristics of IGH CDR3 repertoires for naive, CD27^{dull}, and CD27^{bright} MBCs analyzed using VDJtools software. Besides CDR3 length, all characteristics were calculated for the 5 amino acid residues in the middle of CDR3. KF, Kidera factor. KFs with significant differences between the subsets are shown. KF2, side-chain size; KF3, extended structure preference; KF4, hydrophobicity; KF6, partial specific volume; KF7, flat extended preference. *$p \leq 0.05$, **$p < 0.01$, and ***$p < 0.001$, Tukey's honest significant difference test.

(B) Proportion of isotype usage within naive (N), CD27^{dull} (D), and CD27^{bright} (B) B cells, measured from RNA-seq data using Kallisto software. Statistical significances were tested using two-tailed Student's t tests with Benjamini-Hochberg correction: *$p \leq 0.05$, **$p < 0.01$, ***$p < 0.001$. Note significant differences between CD27^{dull} and CD27^{bright} MBCs. For all isotypes, difference between N, D, and B, p = 7.7e-17 [two-way ANOVA, log(proportion of isotype)]. For all isotypes, difference between D and B, p = 0.02 [two-way ANOVA, log(proportion of isotype)]. Errors bars represent 95% confidence interval.

(C) SM frequencies for the naive (N), CD27^{dull} (D), and CD27^{bright} (B) B cells IG repertoires, showing a higher mutation load for CD27^{bright} compared to CD27^{dull} MBCs (p = 0.01 for ALL, p = 0.002 for IgG, p = 0.02 for IgM, and no significant difference for IgA).

(D) Replacement-to-silent (R:S) mutations ratio for CD27^{bright} (B) and CD27^{dull} (D) MBCs compared between donors for each isotype and total Igs. Using Tukey's honest significant difference test, p = 0.02 for IgG (differences were non-significant for other isotypes). Errors bars are the 95% confidence interval.

(E) Density of replacement and silent SMs by donor and subset for all isotypes.

would shape CDR3 repertoires sufficiently to result in significant differences between naive and $CD27^{dull}$ subsets, as well as between $CD27^{dull}$ and $CD27^{bright}$ subsets.

In line with these considerations, sequential changes were also observed in the relative frequency of isotype usage among the three subsets (Figure 5B). From naive B cells to $CD27^{dull}$ and to $CD27^{bright}$ subsets, the proportions of IgG1, IgG2, IgG4, IgGP, IgA1, and IgA2 isotypes gradually increased, while the proportions of IgM and IgD isotypes decreased. Significant differences in isotype usage frequencies suggest deeper differentiation of $CD27^{bright}$ compared to $CD27^{dull}$ MBCs.

Finally, analysis of mutational load demonstrated that although VH repertoires of both $CD27^{dull}$ and $CD27^{bright}$ subsets are hypermutated, $CD27^{bright}$ MBCs are characterized with a higher density of mutations within both IgG and IgM isotypes (Figure 5C). There is also a higher ratio of replacement-to-silent (R:S) mutations in $CD27^{bright}$ MBCs compared to $CD27^{dull}$ MBCs, confirming that $CD27^{bright}$ MBCs have been more strongly shaped by Ag selection. Within the IgG isotype, the difference between the R:S ratio of $CD27^{dull}$ compared to $CD27^{bright}$ MBCs is significant, suggesting that a stringent Ag-driven pressure selects IgG MBCs into the $CD27^{bright}$ pool (Figure 5D). Further evidence for a stronger selective pressure on $CD27^{bright}$ MBCs is also provided by their higher density of R mutations in the Ig portions determining Ag binding (Figure 5E).

Altogether, the results of VH repertoire analysis suggest a stepwise selection and specialization from naive to $CD27^{dull}$ to $CD27^{bright}$ MBCs. Although the latter two subsets are clonally related, observed unidirectional changes support one-way differentiation and perfection of antigenic specificity on the way from the $CD27^{dull}$ to $CD27^{bright}$ MBC subset rather than to-and-fro plasticity of the two subsets.

The Longitudinal Interplay between $CD27^{dull}$ and $CD27^{bright}$ MBCs during and after Pregnancy

In the second trimester (Trim2) and third trimester (Trim3) of pregnancy, the frequency of MBCs declines to ~40% of the normal level (Figure 6A). By comparing 14 age-matched control non-pregnant women to 11 women in the first trimester, 12 in the second trimester, and 28 in the third trimester of pregnancy, we found that only $CD27^{bright}$ MBCs are significant reduced in the second and third trimesters (Figure 6B).

The loss of MBCs in the PB is a major change, questioning whether the modifications of the B cell compartment associated to pregnancy persist after delivery. We measured $CD27^{dull}$ and $CD27^{bright}$ MBCs in 62 mothers of healthy neonates as well as 48 mothers of children with pertussis and 36 mothers of neonates with lower respiratory tract infections (LRTIs) of viral origin. Samples were collected from all women 1–3 months post-partum. We have shown that the mothers of children with pertussis were themselves infected and reacted to the infection producing pertussis-specific MBCs and Abs (Fedele et al., 2017; Marcellini et al., 2017).

We found that between 1 and 3 months after delivery, MBC frequencies were restored to pre-pregnancy values (Figures 6C and S7), with the $CD27^{dull}$ MBCs showing the largest increase (Figure 6D). In mothers of children with pertussis or LRTIs, the frequency of $CD27^{bright}$ MBCs was significantly higher than in the mothers of healthy neonates (Figure 6D), indicating that maternal exposure to infection drives faster development of $CD27^{bright}$ MBCs.

The rapid recovery of MBC frequencies after pregnancy is surprising, because the generation of MBCs is a long process driven by the antigenic experience of each individual.

Seeking better definition of the changes occurring in the MBC pool during and after pregnancy, we analyzed VH usage and clonal distribution of sorted naive, $CD27^{dull}$, and $CD27^{bright}$ MBCs in the second and third trimesters of pregnancy and 3 months after delivery in three subjects with a physiological pregnancy. The heatmap shows that naive B cells of different women cluster together and are separated from MBCs (Figure 6E), as also observed for HC (Figure 4A). In contrast, VH usage of $CD27^{dull}$ and $CD27^{bright}$ MBCs is individual specific, and individual VH selection is maintained at the three time points (Figure 6E).

Thanks to the identification of $CD27^{dull}$ and $CD27^{bright}$ MBC subsets performed herein, we found that although VH usage remained stable, the relative proportion of $CD27^{dull}$ and $CD27^{bright}$ clonotype variants changed. Indeed, in the identified immunoglobulin (IG) lineage trees (clones) of all three women, we observed a significant decrease in mean clone size for $CD27^{bright}$ MBCs ($p < 10^{-27}$) and increase for $CD27^{dull}$ MBCs ($p < 10^{-13}$) (Figure 6F).

Thus, the results obtained by studying IG lineage trees confirm the loss of $CD27^{bright}$ MBCs in the third trimester (Figures 6B and 6F).

We asked whether the changes in the frequency of $CD27^{dull}$ and $CD27^{bright}$ MBCs in the individual lineage trees could be associated with transitions between these two populations. This likelihood is assessed by representing transitions between and within B cell subsets across time points as 2 × 2 heatmaps (Figure 6G). We found that the reduction of MBC frequency that occurs in pregnancy is combined with a dynamic process where $CD27^{dull}$ MBCs convert into $CD27^{bright}$ MBCs during the second and third trimesters, after pregnancy transitions become less frequent (Figure 6G). Although the mother has a reduced frequency of MBCs at the end of the third trimester, she does not lose her immunological experience, thanks to the maintenance and expansion of persisting clones after delivery (white bars, Figure 6H). In summary, $CD27^{dull}$ MBCs act as a substrate for the conversion into $CD27^{bright}$ MBCs (as shown in the second and third trimesters) and re-expand to replenish MBCs when needed, as after pregnancy.

DISCUSSION

We have presented results that identify key effectors of the human memory response and the strategic behaviors that shape successful immunity. We describe two types of MBCs in the PB with distinct developmental requirements and functions. $CD27^{dull}$ MBCs can be generated without T cell cooperation and in the absence of GC, and $CD27^{bright}$ MBCs obligatorily develop in the GC. The relative abundance of the two subsets changes over the lifetime, with $CD27^{dull}$ being more abundant in infants and $CD27^{bright}$ being the largest population in the elderly.

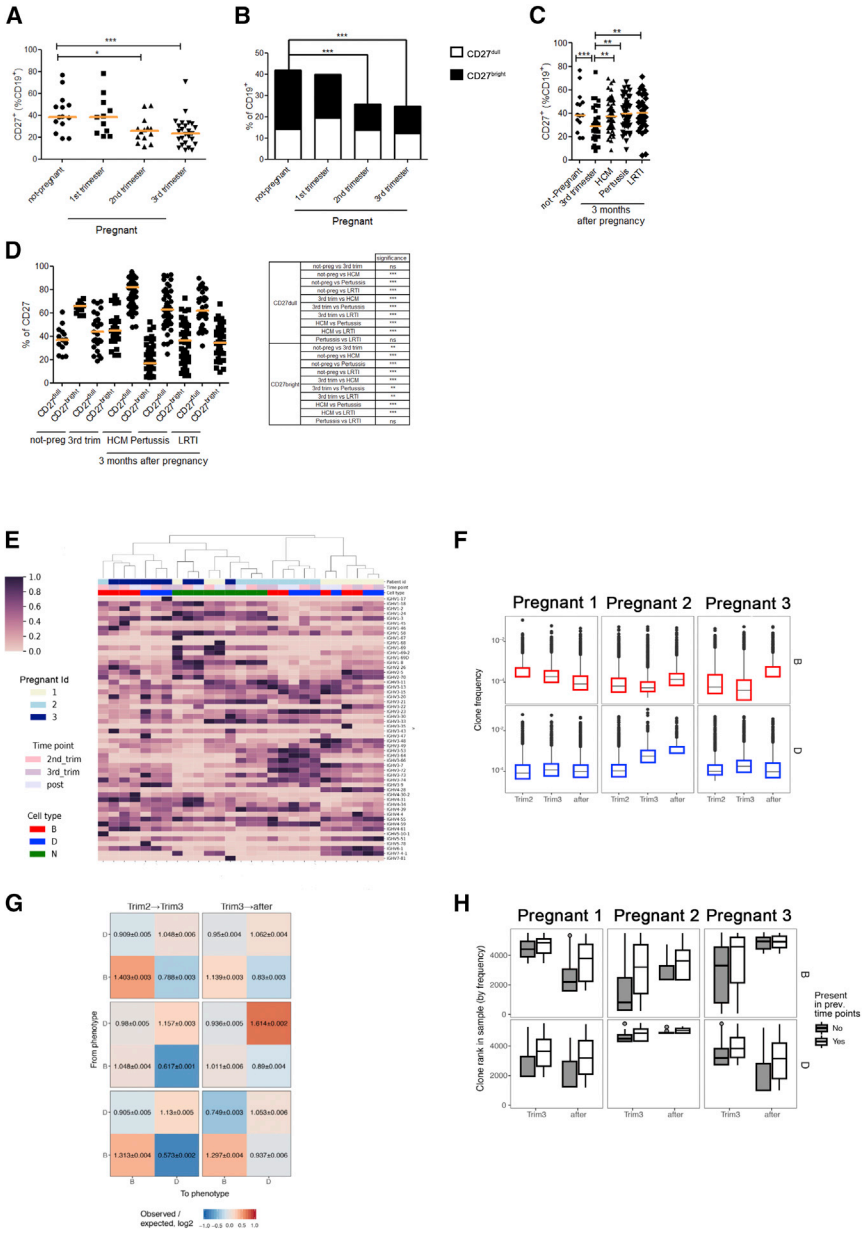

Figure 6. B Cell Clonal Evolution and Subset Transition Analysis in Pregnant Donors

(A and B) Frequencies of B cell subsets among CD19^{+} B cells in the PBMCs of healthy women controls (non-pregnant) and pregnant women during the first (6–11 weeks), second (15–26 weeks), and third (27–38 weeks) trimesters.

(A) Total MBC frequencies.

(B) Percentage of CD27^{dull} (white) and CD27^{bright} (black) MBCs. Statistical differences shown refer to CD27^{bright} MBCs.

(C) Frequencies of CD27^{+} MBCs among CD19^{+} B cells in the PBMCs of not-pregnant women, women in the third trimester of pregnancy, healthy mothers (HCM), mothers of neonates with pertussis (Pertussis), and mothers of neonates with LRTIs analyzed 1–3 months after delivery.

(D) Distribution of CD27^{dull} and CD27^{bright} MBCs within the CD27^{+} MBC compartment in the indicated groups.

(E–H) VH usage and clonal distribution in MBCs from three subjects at the second (Trim2) and third trimesters (Trim3) of pregnancy and 3 months post-partum.

(E) IGHV gene segments usage, weighed (per cDNA molecule). Note co-clustering of naive B cells repertoires of different pregnant women at different time points and co-clustering of CD27^{dull} and CD27^{bright} MBCs.

(F) Distribution of clone sizes (fraction of reads in the sample) at different time points; input of CD27^{bright} and CD27^{dull} reads are calculated separately. A decrease in mean clone size is observed for the CD27^{bright} subset ($p < 10^{-27}$ for all donors, two-tailed t test for log frequencies), while an increase in clone size is observed for the CD27^{dull} subset ($p < 10^{-13}$ for all donors) between the second and third trimesters. Errors bars represent 95% confidence interval.

(G) Transitions between and within MBC subsets across time points shown as 2 × 2 heatmaps. The ratio of observed-to-expected transition counts between and within B and D subsets is shown; the latter is computed as the product of row and column sums divided by the total count of each heatmap. Only transitions in which the parent clonotype occurs in a previous time point and has fewer mutations and its child clonotype is observed at the next time point with more mutations are counted; both clonotypes should belong to the same B cell clone based on lineage analysis. Odds ratios for subset transition, computed as #D→B/#D→D for CD27^{dull} MBCs and #B→D/#B→B, show that CD27^{dull} MBCs are more likely to change the subset than CD27^{bright} ones in second→third trimesters ($p = 0.009$, mean difference in odds ratios is 0.31, paired t test across donors), but not in the third trimester→post-delivery ($p = 0.755$). (H) Rank distribution for persistent (white bars) and emergent (gray bars) lineage trees. Persistent clones of both CD27^{bright} (B) and CD27^{dull} (D) subsets that were observed in the second and third trimesters increase their frequency rank in the third trimester ($p < 0.05$ for B and $p < 10^{-5}$ for D for all donors, two-tailed t test). To eliminate large numbers of tied frequency values, lineage trees with only one read have been omitted. Errors bars represent 95% confidence interval.

(A and B) Numbers of donors were as follows: HD, n = 14; first trimester, n = 11; second trimester, n = 12; third trimester, n = 28. (C and D) Numbers of donors were as follows: HD, n = 14, third trimester, n = 28; HCM, n = 62; pertussis, n = 48; LTRIs, n = 36). Midlines show medians. Statistical significances were determined by unpaired, two-tailed Mann-Whitney *U* tests (**$p < 0.01$ and ***$p < 0.001$).

MBCs are indispensable to the prevention of re-infection (Kurosaki et al., 2015) through the rapid production of high-affinity Abs. We show that CD27^{bright} MBCs are equipped to perform this job thanks to the expression of highly mutated Abs that have the molecular imprints of more pronounced Ag selection than their CD27^{dull} MBC counterparts. In both transcriptome and *in vitro* function, members of the CD27^{bright} subset demonstrate their capacity to differentiate rapidly into ASCs. Thus, CD27^{bright} MBCs, independent of their expressed isotype (IgM, IgG, or IgA), are the powerful effectors of immunological memory.

CD27^{dull} MBCs have fewer SMs and a lower ability to become ASCs and on the differentiation pathway are an intermediate between naive B cells and CD27^{bright} MBCs.

Within interspersed hypermutation trees, CD27^{dull} IGH variants were distributed closer to the roots, supporting the concept that CD27^{dull} cells may serve as a long-lived recruitment substrate for the generation of CD27^{bright} MBCs, which continue their evolution toward maximal specificity to encountered Ags.

MBCs of young children have few or no SMs (Aranburu et al., 2017). We have called such MBCs "innate," because they express Igs that are encoded in the germline and have been selected by the co-evolution of humans with the environmental pathogens and commensals rather than by specific Ags. Innate MBCs are remodeled in the GC, acquiring more SMs (Aranburu et al., 2017). The immune reaction to malaria confirms that Ig germline genes are selected by endemic pathogens in the exposed human populations. Their specificity is further improved by the acquisition of SMs (Krishnamurty et al., 2016; Pieper et al., 2017; Triller et al., 2017). Similarly, MBCs of infants infected with respiratory syncytial virus express neutralizing Abs encoded in the germline that are modified by SMs in older children, thus acquiring increasing affinity (Goodwin et al., 2018).

Our VH repertoire analysis of four HDs showed that within individuals, CD27^{dull} and CD27^{bright} MBCs share a VH repertoire that is different from the repertoire of naive B cells, suggesting that CD27^{dull} MBCs act as a still-plastic source of highly specialized and differentiated CD27^{bright} MBCs. Confirmation of this function as a long-lived substrate for CD27^{bright} MBCs is provided by the results of our longitudinal study in three pregnant women over a period of 9 months, showing the transition of MBCs from the CD27^{dull} to the CD27^{bright} stage between the second and third trimesters.

It is already known that in both mouse and human, IgM-expressing MBCs increasingly accumulate SMs with re-immunization or re-infection (Krishnamurty et al., 2016; Pape et al., 2011; Wendel et al., 2017). Based on the data in the current report, we suggest that the increased Ag specificity is associated with the CD27^{dull} to CD27^{bright} conversion.

In the mouse, primary immune responses generate high-affinity MBCs from naive B cells in the GC (McHeyzer-Williams and McHeyzer-Williams, 2005). During secondary responses, MBCs expressing IgM enter the GC and differentiate into PBLs and switched MBCs (Dogan et al., 2009; Kenderes et al., 2018; Purtha et al., 2011; Pape and Jenkins, 2018). Here, we show that as suggested before (Mascola and Haynes, 2013; Victora and Wilson, 2015), a similar strategy guarantees and preserves B cell memory in human. We demonstrate that the human MBC compartment is composed of a preformed CD27^{dull} pool of MBCs with a selected repertoire from which exceptionally good MBCs are chosen to become CD27^{bright} memory effectors. CD27^{dull} MBCs may enter the GC reaction in competition with naive B cells, having the advantage of a more appropriate transcriptome, increased ability to express AID, and propensity for Ab secretion. Our model for this strategy is presented schematically in Figure 7.

We found that CD27^{dull} MBCs are reduced in elderly people, thus depriving them of the recruitment substrate for the generation of CD27^{bright} MBCs in response to novel infections. In elderly people, naive B cells may be the only cell type available for the immune response to pathogens never encountered before. The reduction of CD27^{dull} MBCs may explain the restricted repertoire of MBCs associated with the increased incidence and severity of infections in the elderly (Janssens and Krause, 2004). Asplenic individuals of all ages have reduced numbers of MBCs expressing IgM (Piano Mortari et al., 2017; Rosado et al., 2013). We show here that both CD27^{dull} and CD27^{bright} MBCs are reduced, confirming our hypothesis that the spleen is necessary for the generation and remodeling of IgM MBCs (Aranburu et al., 2017). Asplenic subjects have an increased susceptibility to infection and sepsis, mostly caused by encapsulated bacteria (Piano Mortari et al., 2017; Price et al., 2007) such as pneumococcus. As susceptibility to pneumococcal infection is also high in the elderly (Janssens and Krause, 2004), CD27^{dull} MBCs may play a fundamental role in initial, potentially T cell-independent immune responses (Kruetzmann et al., 2003; Rosado et al., 2013). Because of the reduction of CD27^{dull} MBCs, elderly and asplenic individuals are forced to generate MBCs from naive B cells in the GC. The use of this pathway (Figure 7A) explains the protective efficacy of T-dependent vaccines in these two categories of individuals.

The origin of CD27^{dull} MBCs is still unclear, but TLR cross-linking may be the T cell- and GC-independent mechanism triggering their development from transitional B cells (Aranburu et al., 2010; Capolunghi et al., 2008). However they arise, we show here that Ig remodeling of innate MBCs initiates at the CD27^{dull} stage.

Immunological memory protects not only the individual but also the species through the placental transfer of maternal Abs that prevent and control infections in the neonate (Zinkernagel, 2001). We show that in the second and third trimesters of pregnancy, CD27^{+} MBCs in the maternal blood are diminished by half due to shrinkage of the CD27^{bright} population (Figures 6A and 6B). Between the second and third trimesters of pregnancy, MBC numbers and VH usage remain stable, but the composition of the MBC compartment is altered (Figure 6), because CD27^{dull} MBCs convert into CD27^{bright} cells. We hypothesize that the reduction of CD27^{bright} MBCs in the PB may be associated with their further development into PBLs to increase the level of maternal Abs (Pou et al., 2019) to be transferred to the child (Figure 7B). The patrimony of protection generated by the mother in her lifetime is thus used to improve the survival chances of the neonate yet is not lost for the woman. After delivery, CD27^{dull} members of preexisting MBC clones expand, thus maintaining the repertoire and the cell numbers of maternal MBCs. In all three women studied, the transition of MBCs from the CD27^{dull} to the CD27^{bright} stage was observed between the second and third trimesters, but not between third trimester and 3 months post-delivery, suggesting that second to third trimester differences are pregnancy specific. In contrast, the differences between the third trimester and 3 months post-delivery may be individual, depending on the personal environment and antigenic exposure. Further studies will identify the triggers and molecular mechanisms driving the changes in the maternal MBC compartment.

The three women included in our study were healthy and did not have infections either during or after pregnancy. We do not know whether exposure to infection would increase the frequency of emerging clones, which are rare in our donors. We did, however, observe that CD27^{bright} MBCs increase when

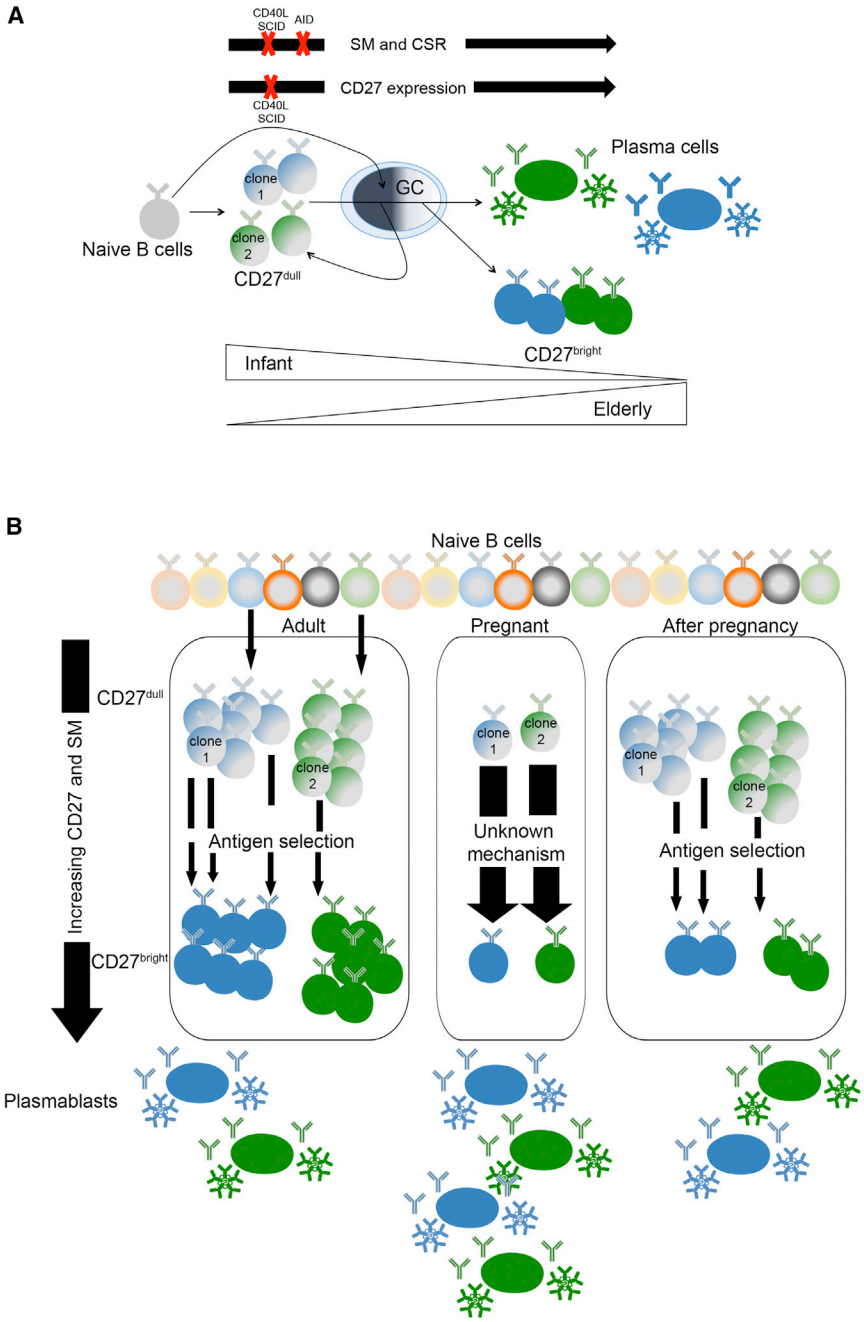

Figure 7. Model of CD27^{dull} and CD27^{bright} MBCs in Humans

(A) MBCs are CD27^{dull} in infancy. They can be generated in patients unable to form GC (SCID, CD40L deficiency). Progression to the CD27^{bright} stage requires the presence and function of the GC, where B cells acquire SMs and undergo CSR. CD27^{dull} MBCs of the adult have more SMs than those produced in children and patients affected by primary immune deficiency, suggesting that CD27^{dull} MBCs may repeat the GC experience more than once and undergo several rounds of selection. CD27^{bright} MBCs are mostly generated from preexisting CD27^{dull} MBCs and express highly mutated B-cell receptors (BCRs) shaped by Ag selection. It is possible that emerging clones also arise from naive B cells entering the GC and directly differentiating into CD27^{bright} MBCs. CD27^{bright} MBCs are closer to the PC stage. In the elderly, most MBCs are CD27^{bright}.

(B) Naive B cells have a diverse VH repertoire. In contrast, CD27^{dull} and CD27^{bright} MBCs have a more restricted and similar VH usage. VH repertoire analysis shows that MBCs of adults are composed of clones containing both CD27^{dull} and CD27^{bright} members and that transitions from the CD27^{dull} to the CD27^{bright} MBC pool occur throughout life. Transitions (arrow) are more likely to occur between the second and third trimesters of pregnancy when the MBC compartment is reduced in size. The diminished frequency of CD27^{bright} MBCs may be associated with their further differentiation into PBLs to fulfill the increased need of Abs to be transferred to the fetus for its protection after birth. After pregnancy, the MBC pool is composed of expanding clones persisting from the third trimester.

mothers are exposed to pertussis infection after delivery, since we had determined previously that these women were infected by pertussis and had increased pertussis-specific MBCs and Abs. CD27^{bright} MBCs also increased in the mothers of neonates with LRTIs, suggesting that the response to infections is always associated to the transition from the CD27^{dull} to CD27^{bright} stage (Fedele et al., 2017; Marcellini et al., 2017).

Our results show that in pregnancy, the immune system of the mother undergoes complex changes, initiating events that will continue after birth when the immune systems of mother and child (Laserson et al., 2014) co-evolve as they adapt to the same environment. During pregnancy, the MBC compartment reacts to still-unknown factors associated with the presence of the fetus that causes two phenomena: (1) the transition from the CD27^{dull} stage to the CD27^{bright} stage (Figure 6G) and (2) a reduction in the CD27^{bright} MBC frequency (Figures 6B and 6F). This occurs at a time when increased levels of maternal Abs are needed for the child.

In each individual, the establishment of the MBC pool takes years (Figure 1A). Instead of regenerating her MBCs *de novo*, after pregnancy, the mother re-expands her CD27^{dull} pool. This strategy has the advantage of maintaining the woman's immunological experience and also the ability to adapt to new cues and Ags. The increase of CD27^{bright} MBCs in mothers with pertussis or LRTIs suggests that the transition from CD27^{dull} to CD27^{bright} is driven by infection and represents the physiologic immune response (Figure 6D).

In summary, the extraordinary situation created in pregnancy by the presence of a fetus has revealed that the strategy of the human MBC response is based on the presence of a CD27^{dull} MBC pool with the capacity to replenish itself and supply cells

that differentiate into CD27^{bright} MBCs. Because of this strategy, the MBC repertoire never loses the patrimony of immunological experience generated by the reaction to infections and vaccinations throughout life. Thus, human B cell memory is essentially stable for each individual, remaining capable of adaptation to antigenic challenges (Laserson et al., 2014). The interrelationship between CD27^{dull} and CD27^{bright} MBC explains the resilience and rapidity of the adult immune response. It remains to be explored whether the establishment of CD27^{dull} MBCs specific for the influenza strain encountered early in life may explain the "original antigenic sin" hypothesized in the response to new influenza viruses (Henry et al., 2018). CD27^{dull} MBCs may recognize conserved influenza epitopes preventing the activation of naive B cells and the generation of MBCs and Abs in response to new viruses and vaccines. In mice, it has been shown that IgM MBCs expressing Tbet are "formally stem cells, similar to those described in CD8 memory T cells" (Graef et al., 2014), because they are able to generate different types of more differentiated MBCs (Kenderes et al., 2018). We propose that this function is carried on by CD27^{dull} MBCs in human.

Recently, Ag-specific B cells (ABCs) induced by infection or vaccination (Ellebedy et al., 2016) have been described. Based on our results, ABCs may represent the next step of differentiation of CD27^{bright} MBCs on their way to become PBLs.

The identification of CD27^{dull} and CD27^{bright} MBCs, with separate and complementary roles, provides important information for the evaluation of vaccine responses, design of vaccination protocols, and development of new vaccines for children, elderly individuals, and pregnant women, as well as more generally in the study of immunodeficiency and autoimmunity.

STAR★METHODS

Detailed methods are provided in the online version of this paper and include the following:

- KEY RESOURCES TABLE
- LEAD CONTACT AND MATERIALS AVAILABILITY
- EXPERIMENTAL MODEL AND SUBJECT DETAILS
  - Ethical statement
  - Human samples
- METHOD DETAILS
  - Cell isolation and cell sorting
  - Stimulation and reagents
  - Flow cytometry and antibodies
  - ELISpot
  - RNA extraction and RNA sequencing
  - RNA-Seq bioinformatic analysis
  - IG heavy RNA-based 5′-RACE with unique molecular identifiers (UMI) and sequencing
  - Bioinformatic analysis of IG heavy RNA-based 5′-RACE with unique molecular identifiers (UMI)
  - Real-time PCR
  - PCR amplification, cloning and sequencing of PCR products
  - Mutation and VH gene segment analysis
- QUANTIFICATION AND STATISTICAL ANALYSIS
- DATA AND CODE AVAILABILITY

SUPPLEMENTAL INFORMATION

Supplemental Information can be found online at https://doi.org/10.1016/j.celrep.2020.02.022.

ACKNOWLEDGMENTS

This work was funded by the Italian Ministry of Health (grant RF2013-02358960) and the Associazione Arcobaleno (R.C.). O.G. was supported by personal fellowships from EMBO, the C.M. Lerici Foundation, and the Royal Society of Arts and Sciences in Gothenburg. A.N.D. was supported by the Ministry of Education, Youth and Sports of the Czech Republic (project CEITEC 2020 LQ1601). A.S.O. and D.M.C. were supported by the Russian Science Foundation (project 19-14-00317). We thank the Pertussis Study Group for their contribution.

AUTHOR CONTRIBUTIONS

A.F., Caterina Cancrini, D.V., Viviana Moschese, C.V., F.S., A.P., G.d.V., S.Z., A.E.T., and V.L. collected the samples. E.G. sorted the cells. S.C., Marco Scarsella, A.A., C.B., Cristina Cristofoletti, C.F., E.M., E.P.M., O.G., S.B., and Valentina Marcellini carried out experiments. D.A.S., A.N.D., A.S.O., and Mikhail Shugay performed RNA-seq analysis and RepSeq analysis. A.G., F.L., M.T., and G.R. contributed significantly to the intellectual content of the paper. E.M., E.P.M., O.G., and R.C. designed the experiments and interpreted the results. E.P.M., O.G., D.M.C., and R.C. wrote the manuscript.

DECLARATION OF INTERESTS

The authors declare no competing interests.

Received: October 18, 2019
Revised: December 23, 2019
Accepted: February 5, 2020
Published: March 3, 2020

REFERENCES

Aranburu, A., Ceccarelli, S., Giorda, E., Lasorella, R., Ballatore, G., and Carsetti, R. (2010). TLR ligation triggers somatic hypermutation in transitional B cells inducing the generation of IgM memory B cells. J. Immunol. *185*, 7293–7301.

Aranburu, A., Piano Mortari, E., Baban, A., Giorda, E., Cascioli, S., Marcellini, V., Scarsella, M., Ceccarelli, S., Corbelli, S., Cantarutti, N., et al. (2017). Human B-cell memory is shaped by age- and tissue-specific T-independent and GC-dependent events. Eur. J. Immunol. *47*, 327–344.

Bernasconi, N.L., Onai, N., and Lanzavecchia, A. (2003). A role for Toll-like receptors in acquired immunity: up-regulation of TLR9 by BCR triggering in naive B cells and constitutive expression in memory B cells. Blood *101*, 4500–4504.

Bolotin, D., Poslavsky, S., Mitrophanov, I., Shugay, M., Mamedov, I.Z., Putintseva, E.V., and Chudakov, D.M. (2015). MiXCR: software for comprehensive adaptive immunity profiling. Nat. Methods *12*, 380–381.

Capolunghi, F., Cascioli, S., Giorda, E., Rosado, M.M., Plebani, A., Auriti, C., Seganti, G., Zuntini, R., Ferrari, S., Cagliuso, M., et al. (2008). CpG drives human transitional B cells to terminal differentiation and production of natural antibodies. J. Immunol. *180*, 800–808.

Colonna-Romano, G., Bulati, M., Aquino, A., Pellicanò, M., Vitello, S., Lio, D., Candore, G., and Caruso, C. (2009). A double-negative (IgD-CD27-) B cell population is increased in the peripheral blood of elderly people. Mech. Ageing Dev. *130*, 681–690.

Dogan, I., Bertocci, B., Vilmont, V., Delbos, F., Mégret, J., Storck, S., Reynaud, C.-A., and Weill, J.-C. (2009). Multiple layers of B cell memory with different effector functions. Nat. Immunol. *10*, 1292–1299.

Ellebedy, A.H., Jackson, K.J.L., Kissick, H.T., Nakaya, H.I., Davis, C.W., Roskin, K.M., McElroy, A.K., Oshansky, C.M., Elbein, R., Thomas, S., et al.

(2016). Defining antigen-specific plasmablast and memory B cell subsets in human blood after viral infection or vaccination. Nat. Immunol. *17*, 1226–1234.

Faas, M.M., Spaans, F., and De Vos, P. (2014). Monocytes and macrophages in pregnancy and pre-eclampsia. Front. Immunol. *5*, 298.

Fedele, G., Carollo, M., Palazzo, R., Stefanelli, P., Pandolfi, E., Gesualdo, F., Tozzi, A.E., Carsetti, R., Villani, A., Nicolai, A., et al. (2017). Parents as source of pertussis transmission in hospitalized young infants. Infection *45*, 171–178.

Fischer, A. (2000). Severe combined immunodeficiencies (SCID). Clin. Exp. Immunol. *122*, 143–149.

Goodwin, E., Gilman, M.S.A., Wrapp, D., Chen, M., Ngwuta, J.O., Moin, S.M., Bai, P., Sivasubramanian, A., Connor, R.I., Wright, P.F., et al. (2018). infants infected with respiratory syncytial virus generate potent neutralizing antibodies that lack somatic hypermutation. Immunity *48*, 339–349.e5.

Graef, P., Buchholz, V.R., Stemberger, C., Flossdorf, M., Henkel, L., Schiemann, M., Drexler, I., Höfer, T., Riddell, S.R., and Busch, D.H. (2014). Serial transfer of single-cell-derived immunocompetence reveals stemness of CD8(+) central memory T cells. Immunity *41*, 116–126.

Henry, C., Palm, A.E., Krammer, F., and Wilson, P.C. (2018). From original antigenic sin to the universal influenza virus vaccine. Trends Immunol. *39*, 70–79.

Janssens, J., and Krause, K. (2004). Pneumonia in the very old. Lancet Infect. Dis. *4*, 112–124.

Kenderes, K.J., Levack, R.C., Papillion, A.M., Cabrera-Martinez, B., Dishaw, L.M., and Winslow, G.M. (2018). T-Bet^{+} IgM memory cells generate multi-lineage effector B cells. Cell Rep. *24*, 824–837.e3.

Klein, U., Rajewsky, K., and Küppers, R. (1998). Human immunoglobulin (Ig) M+IgD+ peripheral blood B cells expressing the CD27 cell surface antigen carry somatically mutated variable region genes: CD27 as a general marker for somatically mutated (memory) B cells. J. Exp. Med. *188*, 1679–1689.

Kosmrlj, A., Jha, A.K., Huseby, E.S., Kardar, M., and Chakraborty, A.K. (2008). How the thymus designs antigen-specific and self-tolerant T cell receptor sequences. Proc. Natl. Acad. Sci. USA *105*, 16671–16676.

Krishnamurty, A.T., Thouvenel, C.D., Portugal, S., Keitany, G.J., Kim, K.S., Holder, A., Crompton, P.D., Rawlings, D.J., and Pepper, M. (2016). Somatically hypermutated plasmodium-specific IgM(+) memory B cells are rapid, plastic, early responders upon malaria rechallenge. Immunity *45*, 402–414.

Kruetzmann, S., Rosado, M.M., Weber, H., Germing, U., Tournilhac, O., Peter, H.-H., Berner, R., Peters, A., Boehm, T., Plebani, A., et al. (2003). Human immunoglobulin M memory B cells controlling Streptococcus pneumoniae infections are generated in the spleen. J. Exp. Med. *197*, 939–945.

Kurosaki, T., Kometani, K., and Ise, W. (2015). Memory B cells. Nat. Rev. Immunol. *15*, 149–159.

Laserson, U., Vigneault, F., Gadala-Maria, D., Yaari, G., Uduman, M., Vander Heiden, J.A., Kelton, W., Taek Jung, S., Liu, Y., Laserson, J., et al. (2014). High-resolution antibody dynamics of vaccine-induced immune responses. Proc. Natl. Acad. Sci. USA *111*, 4928–4933.

Li, H., Handsaker, B., Wysoker, A., Fennell, T., Ruan, J., Homer, N., Marth, G., Abecasis, G., and Durbin, R.; 1000 Genome Project Data Processing Subgroup (2009). The Sequence Alignment/Map format and SAMtools. Bioinformatics *25*, 2078–2079.

Liao, Y., Smyth, G.K., and Shi, W. (2014). featureCounts: an efficient general purpose program for assigning sequence reads to genomic features. Bioinformatics *30*, 923–930.

Lima, J., Martins, C., Leandro, M.J., Nunes, G., Sousa, M.J., Branco, J.C., and Borrego, L.M. (2016). Characterization of B cells in healthy pregnant women from late pregnancy to post-partum: a prospective observational study. BMC Pregnancy Childbirth *16*, 139.

Longo, N.S., Lugar, P.L., Yavuz, S., Zhang, W., Krijger, P.H.L., Russ, D.E., Jima, D.D., Dave, S.S., Grammer, A.C., and Lipsky, P.E. (2009). Analysis of somatic hypermutation in X-linked hyper-IgM syndrome shows specific deficiencies in mutational targeting. Blood *113*, 3706–3715.

Love, M.I., Huber, W., and Anders, S. (2014). Moderated estimation of fold change and dispersion for RNA-seq data with DESeq2. Genome Biol. *15*, 550.

Marasco, E., Farroni, C., Cascioli, S., Marcellini, V., Scarsella, M., Giorda, E., Piano Mortari, E., Leonardi, L., Scarselli, A., Valentini, D., et al. (2017). B-cell activation with CD40L or CpG measures the function of B-cell subsets and identifies specific defects in immunodeficient patients. Eur. J. Immunol. *47*, 131–143.

Marcellini, V., Piano Mortari, E., Fedele, G., Gesualdo, F., Pandolfi, E., Midulla, F., Leone, P., Stefanelli, P., Tozzi, A.E., and Carsetti, R.; Pertussis Study Group (2017). Protection against pertussis in humans correlates to elevated serum antibodies and memory B cells. Front. Immunol. *8*, 1158.

Mascola, J.R., and Haynes, B.F. (2013). HIV-1 neutralizing antibodies: understanding nature's pathways. Immunol. Rev. *254*, 225–244.

McHeyzer-Williams, L.J., and McHeyzer-Williams, M.G. (2005). Antigen-specific memory B cell development. Annu. Rev. Immunol. *23*, 487–513.

Miyazawa, S., and Jernigan, R.L. (1996). Residue-residue potentials with a favorable contact pair term and an unfavorable high packing density term, for simulation and threading. J. Mol. Biol. *256*, 623–644.

Moir, S., Ho, J., Malaspina, A., Wang, W., DiPoto, A.C., O'Shea, M.A., Roby, G., Kottilil, S., Arthos, J., Proschan, M.A., et al. (2008). Evidence for HIV-associated B cell exhaustion in a dysfunctional memory B cell compartment in HIV-infected viremic individuals. J. Exp. Med. *205*, 1797–1805.

Nakada, D., Oguro, H., Levi, B.P., Ryan, N., Kitano, A., Saitoh, Y., Takeichi, M., Wendt, G.R., and Morrison, S.J. (2014). Oestrogen increases haematopoietic stem-cell self-renewal in females and during pregnancy. Nature *505*, 555–558.

Pape, K., and Jenkins, M. (2018). Do memory B cells form secondary germinal centers? It depends. Cold Spring Harb. Perspect. Biol. *10*, a029116.

Pape, K.A., Taylor, J.J., Maul, R.W., Gearhart, P.J., and Jenkins, M.K. (2011). Different B cell populations mediate early and late memory during an endogenous immune response. Science *331*, 1203–1207.

Parham, P. (2004). NK cells and trophoblasts: partners in pregnancy. J. Exp. Med. *200*, 951–955.

Patel, R.K., and Jain, M. (2012). NGS QC Toolkit: a toolkit for quality control of next generation sequencing data. PLoS ONE *7*, e30619.

Piano Mortari, E., Baban, A., Cantarutti, N., Bocci, C., Adorisio, R., and Carsetti, R. (2017). Heterotaxy syndrome with and without spleen: different infection risk and management. J. Allergy Clin. Immun. *139*, 1981–1984.e1.

Pieper, K., Tan, J., Piccoli, L., Foglierini, M., Barbieri, S., Chen, Y., Silacci-Fregni, C., Wolf, T., Jarrossay, D., Anderle, M., et al. (2017). Public antibodies to malaria antigens generated by two LAIR1 insertion modalities. Nature *548*, 597–601.

Pou, C., Nkulikiyimfura, D., Henckel, E., Olin, A., Lakshmikanth, T., Mikes, J., Wang, J., Chen, Y., Bernhardsson, A.K., Gustafsson, A., et al. (2019). The repertoire of maternal anti-viral antibodies in human newborns. Nat. Med. *25*, 591–596.

Price, V.E., Blanchette, V.S., and Ford-Jones, E.L. (2007). The prevention and management of infections in children with asplenia or hyposplenia. Infect. Dis. Clin. North Am. *21*, 697–710, viii–ix.

Purtha, W.E., Tedder, T.F., Johnson, S., Bhattacharya, D., and Diamond, M.S. (2011). Memory B cells, but not long-lived plasma cells, possess antigen specificities for viral escape mutants. J. Exp. Med. *208*, 2599–2606.

Quartier, P., Bustamante, J., Sanal, O., Plebani, A., Debré, M., Deville, A., Litzman, J., Levy, J., Fermand, J.P., Lane, P., et al. (2004). Clinical, immunologic and genetic analysis of 29 patients with autosomal recessive hyper-IgM syndrome due to activation-induced cytidine deaminase deficiency. Clin. Immunol. *110*, 22–29.

Revy, P., Muto, T., Levy, Y., Geissmann, F., Plebani, A., Sanal, O., Catalan, N., Forveille, M., Dufourcq-Labelouse, R., Gennery, A., et al. (2000). Activation-induced cytidine deaminase (AID) deficiency causes the autosomal recessive form of the hyper-IgM syndrome (HIGM2). Cell *102*, 565–575.

Roberts, J.L., Lengi, A., Brown, S.M., Chen, M., Zhou, Y.J., O'Shea, J.J., and Buckley, R.H. (2004). Janus kinase 3 (JAK3) deficiency: clinical, immunologic, and molecular analyses of 10 patients and outcomes of stem cell transplantation. Blood *103*, 2009–2018.

Roederer, M. (2011). Interpretation of cellular proliferation data: avoid the panglossian. Cytometry A. *79*, 95–101.

Rosado, M.M., Gesualdo, F., Marcellini, V., Di Sabatino, A., Corazza, G.R., Smacchia, M.P., Nobili, B., Baronci, C., Russo, L., Rossi, F., et al. (2013). Preserved antibody levels and loss of memory B cells against pneumococcus and tetanus after splenectomy: tailoring better vaccination strategies. Eur. J. Immunol. *43*, 2659–2670.

Ruocco, M.G., Chaouat, G., Florez, L., Bensussan, A., and Klatzmann, D. (2014). Regulatory T-cells in pregnancy: historical perspective, state of the art, and burning questions. Front. Immunol. *5*, 389.

Schatorjé, E.J.H., Driessen, G.J., van Hout, R.W.N.M., van der Burg, M., and de Vries, E. (2014). Levels of somatic hypermutations in B cell receptors increase during childhood. Clin. Exp. Immunol. *178*, 394–398.

Segerer, S.E., Staib, C., Kaemmerer, U., Frambach, T., Honig, A., Dietl, J., and Rieger, L. (2012). Dendritic cells: elegant arbiters in human reproduction. Curr. Pharm. Biotechnol. *13*, 1378–1384.

Shugay, M., Britanova, O.V., Merzlyak, E.M., Turchaninova, M.A., Mamedov, I.Z., Tuganbaev, T.R., Bolotin, D.A., Staroverov, D.B., Putintseva, E.V., Plevova, K., et al. (2014). Towards error-free profiling of immune repertoires. Nat. Methods *11*, 653–655.

Shugay, M., Bagaev, D.V., Turchaninova, M.A., Bolotin, D.A., Britanova, O.V., Putintseva, E.V., Pogorelyy, M.V., Nazarov, V.I., Zvyagin, I.V., Kirgizova, V.I., et al. (2015). VDJtools: unifying post-analysis of T cell receptor repertoires. PLoS Comput. Biol. *11*, e1004503.

Stadinski, B.D., Shekhar, K., Gómez-Touriño, I., Jung, J., Sasaki, K., Sewell, A.K., Peakman, M., Chakraborty, A.K., and Huseby, E.S. (2016). Hydrophobic CDR3 residues promote the development of self-reactive T cells. Nat. Immunol. *17*, 946–955.

Suan, D., Kräutler, N.J., Maag, J.L.V., Butt, D., Bourne, K., Hermes, J.R., Avery, D.T., Young, C., Statham, A., Elliott, M., et al. (2017). CCR6 defines memory b cell precursors in mouse and human germinal centers, revealing light-zone location and predominant low antigen affinity. Immunity *47*, 1142–1153.e4.

Tangye, S.G., and Ma, C.S. (2020). Regulation of the germinal center and humoral immunity by interleukin-21. J. Exp. Med. *217*, e20191638.

Triller, G., Scally, S.W., Costa, G., Pissarev, M., Kreschel, C., Bosch, A., Marois, E., Sack, B.K., Murugan, R., Salman, A.M., et al. (2017). Natural parasite exposure induces protective human anti-malarial antibodies. Immunity *47*, 1197–1209.e10.

Turchaninova, M.A., Davydov, A., Britanova, O.V., Shugay, M., Bikos, V., Egorov, E.S., Kirgizova, V.I., Merzlyak, E.M., Staroverov, D.B., Bolotin, D.A., et al. (2016). High-quality full-length immunoglobulin profiling with unique molecular barcoding. Nat. Protoc. *11*, 1599–1616.

Victora, G.D., and Wilson, P.C. (2015). Germinal center selection and the antibody response to influenza. Cell *163*, 545–548.

Wang, S., Wang, J., Kumar, V., Karnell, J.L., Naiman, B., Gross, P.S., Rahman, S., Zerrouki, K., Hanna, R., Morehouse, C., et al.; Autoimmunity Molecular Medicine Team (2018). IL-21 drives expansion and plasma cell differentiation of autoreactive CD11c^{hi}T-bet^{+} B cells in SLE. Nat. Commun. *9*, 1758.

Watson, C.T., Glanville, J., and Marasco, W.A. (2017). The individual and population genetics of antibody immunity. Trends Immunol. *38*, 459–470.

Wei, C., Anolik, J., Cappione, A., Zheng, B., Pugh-Bernard, A., Brooks, J., Lee, E.-H., Milner, E.C.B., and Sanz, I. (2007). A new population of cells lacking expression of CD27 represents a notable component of the B cell memory compartment in systemic lupus erythematosus. J. Immunol. *178*, 6624–6633.

Weller, S., Faili, A., Garcia, C., Braun, M.C., Le Deist F, F., de Saint Basile G, G., Hermine, O., Fischer, A., Reynaud, C.A., and Weill, J.C. (2001). CD40-CD40L independent Ig gene hypermutation suggests a second B cell diversification pathway in humans. Proc. Natl. Acad. Sci. USA *98*, 1166–1170.

Wendel, B.S., He, C., Qu, M., Wu, D., Hernandez, S.M., Ma, K.Y., Liu, E.W., Xiao, J., Crompton, P.D., Pierce, S.K., et al. (2017). Accurate immune repertoire sequencing reveals malaria infection driven antibody lineage diversification in young children. Nat. Commun. *8*, 531.

Wickham, H. (2009). ggplot2: Elegant Graphic for Data Analysis (Springer), pp. 1–210.

Wu, Y.-C.B., Kipling, D., and Dunn-Walters, D.K. (2011). The relationship between CD27 negative and positive B cell populations in human peripheral blood. Front. Immunol. *2*, 81.

Yokota, T., Oritani, K., Sudo, T., Ishibashi, T., Doi, Y., Habuchi, Y., Ichii, M., Fukushima, K., Okuzaki, D., Tomizuka, K., et al. (2015). Estrogen-inducible sFRP5 inhibits early B-lymphopoiesis in vivo, but not during pregnancy. Eur. J. Immunol. *45*, 1390–1401.

Yoshida, T., Mei, H., Dörner, T., Hiepe, F., Radbruch, A., Fillatreau, S., and Hoyer, B.F. (2010). Memory B and memory plasma cells. Immunol. Rev. *237*, 117–139.

Zinkernagel, R.M. (2001). Maternal antibodies, childhood infections, and autoimmune diseases. N. Engl. J. Med. *345*, 1331–1335.

Zotos, D., Coquet, J.M., Zhang, Y., Light, A., D'Costa, K., Kallies, A., Corcoran, L.M., Godfrey, D.I., Toellner, K.-M., Smyth, M.J., et al. (2010). IL-21 regulates germinal center B cell differentiation and proliferation through a B cell-intrinsic mechanism. J. Exp. Med. *207*, 365–378.

Zuccarino-Catania, G.V., Sadanand, S., Weisel, F.J., Tomayko, M.M., Meng, H., Kleinstein, S.H., Good-Jacobson, K.L., and Shlomchik, M.J. (2014). CD80 and PD-L2 define functionally distinct memory B cell subsets that are independent of antibody isotype. Nat. Immunol. *15*, 631–637.

STAR★METHODS

KEY RESOURCES TABLE

REAGENT or RESOURCE	SOURCE	IDENTIFIER
Antibodies		
CD19 (Clone SJ25C1) BUV737	BD Biosciences	Cat#564303; RRID: AB_2716867
CD19 (Clone SJ25C1) APCH7	BD Biosciences	Cat#560177; RRID: AB_1645470
CD19 (Clone HIB19) PECy5	BD Biosciences	Cat#555414; RRID: AB_395814
CD24 (Clone ML5) BV711	BD Biosciences	Cat#5634501; RRID: AB_2738164
CD27 (Clone M-T271) FITC	BD Biosciences	Cat#555440; RRID: AB_395833
CD27 (Clone M-T271) PE	BD Biosciences	Cat#557330; RRID: AB_395834
CD27 (Clone M-T271) APC	BD Biosciences	Cat#555441; RRID: AB_395834
CD27 (Clone L128) BV605	BD Biosciences	Cat#562655; RRID: AB_2744351
CD38 (Clone HB7) PE-Cy7	BD Biosciences	Cat#335790; RRID: AB_399969
CD38 (Clone HIT2) BV421	BD Biosciences	Cat#562445; RRID: AB_11151894
IgM (Polyclonal) Alexa Fluor 647	Jackson Immunoresearch	Cat#109-606-129; RRID: AB_2337901
IgD (Clone IA6-2) FITC	BD Biosciences	Cat#555778; RRID: AB_396113
IgG (Clone G18-145) BUV395	BD Biosciences	Cat#564229; RRID: AB_2738683
IgA (Clone IS11-8E10) FITC	Miltenyi Biotec	Cat#130-113-475; RRID: AB_1036156
CD23 (Clone M-L233) Biotin	BD Biosciences	Cat#555709; RRID: AB_396055
CD200 (Clone MRC OX-104) BV421	BD Biosciences	Cat#564114; RRID: AB_2738602
IL-21R (Clone 17A12) PE	BD Biosciences	Cat#560264; RRID: AB_1645517
CD95 (Clone DX2) PE	BD Biosciences	Cat#555674; RRID: AB_396027
CXCR3 (Clone 1C6/CXCR3) PE	BD Biosciences	Cat#557185; RRID: AB_396596
TCL1 (Clone 1-21) APC	eBioscience	Cat#17-6699-42; RRID: AB_11149309
CD3 (Clone UCHT1) Pacific blue	BD Biosciences	Cat#558117; RRID: AB_397038
CD14 (Clone M5E2) Pacific blue	BD Biosciences	Cat#558121; RRID: AB_397041
CD138 (Clone MI15) PE	BD Biosciences	Cat#552026; RRID: AB_394323
CD45RA (Clone HI100) FITC	BD Biosciences	Cat#555488; RRID: AB_395879
CD45RO (Clone UCHL1) PECy7	BD Biosciences	Cat#337168; RRID: AB_647426
B220 (Clone RA3-6B2) APC	BD Biosciences	Cat#553092; RRID: AB_398531
a4b7 (Clone FIB504) PE	BD Biosciences	Cat#555945; RRID: AB_396241
CXCR4 (Clone 12G5) PE-Cy5)	BD Biosciences	Cat#560937; RRID: AB_2033946
CXCR5 (Clone RF8B2) Alexa Fluor 647	BD Biosciences	Cat#558113; RRID: AB_394324
HLADR (Clone L243) APC-H7	BD Biosciences	Cat#641411; RRID: AB_399991
TACI (Clone 11H3) Biotin	eBioscience	Cat#13-9217-82; RRID: AB_466973
CD127 (Clone HIL-7R-M21) BV786	BD Biosciences	Cat#563324; RRID: AB_2738138
CD80 (Clone L307.4) FITC	BD Biosciences	Cat#557226; RRID: AB_396605
PDL2 (Clone MIH18) PE	BD Biosciences	Cat#558066; RRID: AB_647197
CD10 (Clone HI10a) PE	BD Biosciences	Cat#557143; RRID: AB_396586
CD22 (Clone HIB22) PE-Cy5	BD Biosciences	Cat#555425; RRID: AB_395819
CD86 (Clone 2331 (FUN-1)) PE	BD Biosciences	Cat#557344; RRID: AB_396013
CCR6 (Clone 11A9) PE	BD Biosciences	Cat#561019; RRID: AB_397273
CD21 (Clone B-ly4) PE	BD Biosciences	Cat#557327; RRID: AB_396641
CD11c (B-ly6) PE-Cy5	BD Biosciences	Cat#551077; RRID: AB_394034
Biological Samples		
Human peripheral blood	Bambino Gesù Children Hospital and San Camillo Hospital, Rome, Italy	N/A
Human tonsils	Bambino Gesù Children Hospital	N/A

(*Continued on next page*)

Continued

REAGENT or RESOURCE	SOURCE	IDENTIFIER
Chemicals, Peptides, and Recombinant Proteins		
CFSE	Life Technologies	Cat#C34554
CpG-B ODN 2006	Hycult Biotech	Cat#HC4039
rhCD40L	Enzo Life Sciences	Cat#ALX-522-015-C010
rhIL-21	Peprotech	Cat#200-21
SMARTScribe Reverse Transcriptase	Clontech	Cat#639538
Critical Commercial Assays		
Rneasy Plus Micro Kit	QIAGEN	Cat#74034
Qubit RNA HS Assay Kit	ThermoFisher Scientific	Cat#Q32855
TruSeq RNA Sample Preparation v2 Kit	Illumina	Cat#RS-122-2001
Agencourt AMPure XP beads	Beckman Coulter	Cat#A63880
Agilent DNA 1000 chip	Agilent Technologies	Cat#5067-1504
Qubit dsDNA HS Assay Kit	ThermoFisher Scientific	Cat#Q32854
MiSeq reagent Kit v3 (600 cycles)	Illumina	Cat#MS-102-3003
NextSeq® 500/550 High Output Kit v2 (150 cycles)	Illumina	Cat#TG-160-2002
Deposited Data		
RNA-seq data	NCBI	SRP241753
IGH repertoire in HD	figshare	https://doi.org/10.6084/m9.figshare.11592036
IGH repertoire in pregnancy	figshare	https://doi.org/10.6084/m9.figshare.11592027
Oligonucleotides		
ACTB	IDT	Cat#Hs.PT.39a.22214847
AICDA	IDT	Cat#Hs.PT.53a.976805
ITPR1	IDT	Cat#Hs.PT.58.39512243
TCL-1	IDT	Cat#Hs.PT.58.21038407
TFEC	IDT	Cat#Hs.PT.58.26872107
BAIAP3	ThermoFischer Scientific	Cat#Hs00187529_m1
DUSP4	ThermoFischer Scientific	Cat#Hs01027785_m1
GAPDH	ThermoFischer Scientific	Cat#Hs99999905_m1
PRDM1	ThermoFischer Scientific	Cat#Hs00153357_m1
SPRY1	ThermoFischer Scientific	Cat#Hs01391580_m1
SmartNNNext; AGATGUGTAUAAGAGACAGN NNNUNNNNUNNNNUCTT(rG)4	IDT	N/A
hIGG_r1; GAAGTAGTCCTTGACCAGGCA	IDT	N/A
hIGM_r1; GTGATGGAGTCGGGAAGGAAG	IDT	N/A
hIGA_r1; GCGACGACCACGTTCCCATCT	IDT	N/A
Common primer; AGATGTGTATAAGAGACAG	IDT	N/A
Common-hIGG_r2; AGATGTGTATAAGAGACA GARGGGGAAGACSGATG	IDT	N/A
Common-hIGA_r2; AGATGTGTATAAGAGACA GCAGCGGGAAGACCTTG	IDT	N/A
Common-hIGM_r2; AGATGTGTATAAGAGACA GAGGGGGAAAAGGGTTG	IDT	N/A
F-common; TCGTCGGCAGCGTCAGATGTGTA TAAGAGACAG	IDT	N/A
R- common; GTCTCGTGGGCTCGGAGATGTG TATAAGAGACAG	IDT	N/A

(*Continued on next page*)

Continued		
REAGENT or RESOURCE	SOURCE	IDENTIFIER
Fc_i7; CAAGCAGAAGACGGCATACGAGAT[i7] GTCTCGTGGGCTCGG	Illumina	Cat#FC-121-1011
Fc_i5; AATGATACGGCGACCACCGAGATCTAC AC[i5]TCGTCGGCAGCGTC	Illumina	Cat#FC-121-1011
Software and Algorithms		
FlowJo 10	FLOWJO, LLC	https://www.flowjo.com
Prism 8	GraphPad software	https://www.graphpad.com/scientific-software/prism/
MIGEC software	Shugay et al., 2014	https://github.com/mikessh/migec/releases
MiXCR_v2.1.10	Bolotin et al., 2015	https://github.com/milaboratory/mixcr/releases/tag/v2.1.10
VDJtools_v1.1.8 software	Shugay et al., 2015	https://github.com/mikessh/vdjtools/releases/tag/1.1.8

LEAD CONTACT AND MATERIALS AVAILABILITY

Further information and requests for resources and reagents should be directed to and will be fulfilled by the Lead Contact: Rita Carsetti, rita.carsetti@opbg.net

This study did not generate new unique reagents.

EXPERIMENTAL MODEL AND SUBJECT DETAILS

Ethical statement

Informed consent was obtained for all experiments and the study was performed following the guidelines of the Declaration of Helsinki. The study was approved by the Ethical Committees of Bambino Gesù Children's Hospital and by the San Camillo Hospital.

Human samples

We analyzed PB from anonymous healthy infants (0-1 year), children (3-4 years), toddlers (6-9 years), adults (30-40 years), elderly (75-93 years) and pregnant women. We have no sex information for infants, children, toddlers, adults and elderly. PB of mothers of infants younger than 6 months of age with and without pertussis were collected during a follow-up visit at our hospital (Fedele et al., 2017). Patients with primary immunodeficiencies included in the study were: untransplanted infants, two males with IL-2Receptor Gamma-Chain (*IL2RG*) defects and one male with JAK3 deficiency; two transplanted children (male) with *IL2RG* defects having undergone bone marrow transplantation (without conditional pre-treatment); three patients (male) with CD40L-deficiency and two with AID-deficiency (male). All material from healthy adults were from anonymous buffy coats. Sex information were recorded only for the 4 male subjects analyzed for RNaseq and for the 4 subjects used for RepSeq (3 male and 1 female). Pregnant women were recruited from San Camillo Hospital and from Bambino Gesù Children Hospital in Rome.

METHOD DETAILS

Cell isolation and cell sorting

Heparinized PBMCs were isolated by Ficoll Paque Plus 206 (Amersham PharmaciaBiotech) density-gradient centrifugation. Buffy coats were incubated with RosetteSep human B cell enrichment antibody cocktail (StemCell Technologies, Inc.) and then B cells were isolated by density-gradient centrifugation. B cells were then stained with Abs against CD19, CD24 and CD27 (BD Biosciences). The B cell subsets were gated as follows: mature-naive B cells as $CD24^{+}CD27^{-}$, $CD27^{dull}$ MBCs as $CD24^{+}CD27^{+}$ and $CD27^{bright}$ MBCs as $CD24^{+}CD27^{++}$. Sorting was performed using the FACSAria^{TM} III cell sorter (BD Biosciences). Sort purities were > 99%.

Stimulation and reagents

Naive, $CD27^{dull}$ and $CD27^{bright}$ MBCs were loaded with CFSE (Life Technologies). Briefly, $1x10^{6}$ cells/ml were resuspended in PBS (Euroclone) with 1% FBS (GIBCO BRL) and loaded with 1 μM CFSE for 20 minutes at 37°C. Cells were then washed and stimulated with 0.35 μM TLR9 agonist CpG-B ODN2006 (Hycult Biotech); or 1 μg/mL rhCD40L (Enzo Life Sciences) plus 10 μg/mL anti-IgM/IgG/IgA (Jackson Immunoresearch) and 20 ng/ml rhIL-21 (Peprotech) in complete medium at a concentration of $2.5x10^{6}$ cells/ml.

Complete medium was prepared as follows: RPMI-1640 (Euroclone), 10% heat inactivated fetal bovine serum (FBS, Hyclone Laboratories), 1% L-Glutammine (GIBCO BRL); 1% Penicillin/Streptomicin 100X (Euroclone), 1% sodium pyruvate (GIBCO BRL).

Flow cytometry and antibodies

Cells were stained with the appropriate combination of fluorochrome-conjugated antibodies to identify B cell subsets according to standard techniques. Cells were acquired on a BD LSRFortessa X-20 (BD Biosciences). Data were analyzed with FlowJo ver.8 or 10 (Treestar). Dead cells were excluded from analysis by side/forward scatter gating. Cells were stained with CFSE to measure cell proliferation induced by *in vitro* stimulation. The analysis of CFSE distribution allows the calculation of the proliferation index, corresponding to the mean number of divisions of all cells that have responded. The proliferation index reflects the intrinsic ability of the different cell types to respond to signals. The number of divided cells is the percent of cells that have divided in the final population (Roederer, 2011). Proliferation index and percentage of divided cells were calculated using the proliferation tool provided by FlowJo ver.8

ELISpot

This method has been described in detail previously (Marcellini et al., 2017). In short, AffiniPure F(ab')2 Fragment Goat anti-human IgA+IgG+IgM (H+L) (Jackson ImmunoResearch), synthetic tetanus toxin peptide (C-term) (Acris-antibodies) or PneumoVax (Sanofi Pasteur MSD) were used for coating 96-well plates (MultiScreen-HA, Millipore). PBMCs, naive B cells, $CD27^{dull}$ or $CD27^{bright}$ MBCs stimulated for 5 days with CpG, as described before, were collected, counted, and seeded in the precoated plates. Plates were incubated at 37°C for 3 hours to allow Ab secretion. HPRO-labeled Abs were used for detection: anti-IgM (1:1000), anti-IgG (1:2000) or anti-IgA (1:2000) (Jackson ImmunoResearch) diluted in PBS + gelatin 1% + 0.05% Tween20 (Sigma). TMB substrate (ready to use from Mabtech) was used according to the manufacturer's instructions. Plates were left at room temperature to allow the blue color to develop and the reaction was stopped with ddH_2O. Plates were left to dry before counting with an ELISCAN (A-EL-VIS).

RNA extraction and RNA sequencing

Total RNA was isolated from cells of four HDs (age range 28-48 years) using RNeasy Plus Micro kit (QIAGEN). The concentration of total RNA extracted was quantified using the Qubit® RNA HS Assay Kit (ThermoFischer Scientific). The TruSeq® RNA Sample Preparation v2 Kit (Illumina) was used for isolation of polyadenylated mRNA with oligo-dT beads, second strand cDNA synthesis and NGS library preparation. During the second strand synthesis, dUTP was incorporated in place of dTTP, thus preventing amplification of this strand during the subsequent PCR step and retaining strand information. Unique indexes, included in the standard TruSeq kit set A (Illumina) were incorporated at the adaptor ligation step for multiplex sample loading on the flow cells. The resulting constructs were purified by two consecutive AMPure XP beads cleanup steps and enriched by 15 cycles of PCR. Quality and quantity of the libraries were assessed using an Agilent DNA 1000 chip (Agilent Tecnologies) and Qubit® dsDNA HS Assay Kit, respectively. Libraries were pooled in equimolar amounts (12 libraries/pool) and loaded onto High Output flow cell. The sequencing run was performed in paired-end mode (2 X 76-bp reads) using the Illumina NextSeq 500 platform. Base calling was performed by the instrument computer using Illumina Real Time Analysis (RTA) software that is integrated with NextSeq Control Software (NCS) and provides a summary of quality statistics as per Illumina's acceptance criteria for sequencing. CASAVA 1.8.2 was used for de-multiplexing and conversion of base calls to paired-end FASTQ files.

RNA-Seq bioinformatic analysis

FASTQ files were filtered using NGS QC Toolkit (Patel and Jain, 2012) and low quality reads (phred cutoff of 20 for at least 70% of the read length) and reads with length less than 50 bases were excluded. Cleaned reads were aligned onto the complete GRCh37 human genome by means of HISAT2 (http://ccb.jhu.edu/software/hisat2/index.shtml) providing a list of splice sites from Gencode and RefSeq databases and a list of common SNPs from the dbSNP 147 database. Differential gene expression analysis was conducted by using the DESeq2 R package (Love et al., 2014). Unique and concordant alignments in Sequence Alignment Map (SAM) format were converted to the binary (BAM) format and sorted by genomic coordinates using SAMtools (Li et al., 2009).

Gene expression quantification was performed using featureCounts (Liao et al., 2014) (included in the Subread package), with Gencode 26 (mapped to the GRCh37 assembly) transcriptome annotation, and differential expression test was conducted with DESeq2 (Love et al., 2014) with default parameters.

Graphical representations, including heatmaps of regularized log transformed counts and PCA, were generated with R libraries RColorBrewer and gplots. Plots reporting gene expression as log2 (fold change) were generated by R library ggplot2 (Wickham, 2009).

IG heavy RNA-based 5′-RACE with unique molecular identifiers (UMI) and sequencing

RNA from sorted naive B cells, $CD27^{dull}$ and $CD27^{bright}$ MBCs of 4 HDs (age range 36-51 years) and 3 pregnant women (age range 31-39 years; 3 time points: Trim2, Trim3 and 3 months after delivery) was prepared as described in Turchaninova et al. (2016). Up to 700 ng of total RNA was used for cDNA synthesis. cDNA synthesis primer mix (final concentration 1 μM each) was incubated with RNA (Mix 1) for 4 min at 70°C and then for 2 min at 42°C. To this was added 1X first-strand Buffer (Clontech, final concentration 1X), DTT (SMARTscribe, 2mM), dNTP (1mM each), 10x 5′-Template switch adaptor (1 μM) and SMARTScribe Reverse Transcriptase (Clontech, 10U/ml), and the resulting mix was incubated for 60 min at 42°C. After adding 1 μL of uracil DNA glycosylase (Biolabs, 5 U/μl) and incubating for 40 min at 37°C, cDNA was purified using Agencourt AMPure XP beads (Beckman Coulter).

We then performed a first PCR amplification (95°C for 90 s (1X); 95°C for 10 s, 54°C for 20 s and 72°C for 40 s (18X) and a final step of 4 min at 72°C). In sterile thin-walled 0.2 mL reaction tubes we mixed the following reagents: cDNA from previous step, Q5 polymerase buffer (NEB, final concentration 1x), dNTP mix (0.2 mM each), Q5 polymerase (0.02 U/l), first PCR reverse primer mix (0.4 μM), Common primer (0.4 μM) and nuclease-free water. We used a portion of cDNA equivalent to 50.000 naive B cells and 20.000 MBCs ($CD27^{dull}$ or $CD27^{bright}$). PCR products were purified using the AMPure XD beads and resuspended in 25 μL of elution buffer.

A second PCR amplification was performed (95°C for 90 s (1X); 95°C for 10 s, 54°C for 20 s and 72°C for 40 s (10X) and a final step of 4 min at 72°C). 2 μL of purified product from the first PCR amplification was mixed with Q5 polymerase buffer (NEB, final concentration 1x), dNTP mix (0.2 mM each), Q5 polymerase (0.02 U/μl), forward common primer (0.8 M)reverse common primer (0.8 μM) and Nuclease-free water. As before PCR products were purified with beads and eluted in 20 μl.

Purified DNA from the previous PCR of each sample was mixed with Q5 polymerase buffer (NEB, final concentration 1x), dNTP mix (0.2 mM each), Q5 polymerase (0.02 U/μl), nuclease-free water and a unique combination of Fc_i5 indexed primer 0.2 M and Fc_i7 indexed primer 0.2 M (Nextera index kit, Illumina). PCR was performed using following parameters: 95°C for 90 s (1X); 95°C for 10 s, 60°C for 20 s and 72°C for 40 s (5X) and a final step of 4 min at 72°C. As before PCR products were purified with beads.

For the MiSeq run, we prepared and pooled our libraries by combining equal molar portions of each sample. We spiked the library with 30% of PhiX Control V3 (Illumina). We set the run using symmetric 310+310-nt paired-end Illumina MiSeq sequencing, standard Illumina sequencing primers and MiSeq reagent Kit v3 (600 cycles, Illumina).

Bioinformatic analysis of IG heavy RNA-based 5′-RACE with unique molecular identifiers (UMI)

Demultiplexing, UMI extraction and UMI-based consensus assembling was performed using MIGEC software (Shugay et al., 2014). UMI-based analysis was previously shown to achieve nearly error-free immune repertoires (Shugay et al., 2014; Turchaninova et al., 2016). Multiplex primers to IGHC segments were trimmed to avoid confusions in isotype identification. Further reads mapping and clonotype assembly was performed using MiXCR_v2.1.10 as described previously (Bolotin et al., 2015) with some changes in the MiXCR analysis pipeline (the KAligner alignment algorithm that detects indels of more than 2 nt).

Comparative analysis of IGH repertoire features, such as clonotype overlap and CDR3 physicochemical properties, was performed using VDJtools_v1.1.8 software (Shugay et al., 2015). Allelic variants were identified as the ones supported by at least 5 clonotypes that were present in at least 40% of both molecules and clonotypes with a given Variable segment. They were filtered from the overall pool of detected mutations prior to the analysis of somatic hypermutation frequencies.

Real-time PCR

RNA was quantified and retrotranscribed to cDNA with SuperScript® III Reverse Transcriptase (Invitrogen) following the manufacturer's instructions. All samples were run in triplicate in a 15 μL reaction volume containing 2x TaqMan Universal PCR Master Mix (ThermoFisher Scientific), 20x primers from Integrated DNA Technologies, 25 ng of cDNA and water. The qPCR was run in the Abi Prism 7900 HT Fast Real Time PCR System (ThermoFisher Technologies) using the following amplification parameters: 10 min at 95°C followed by 40 cycles of 15 s at 95°C, and 1 min at 60°C. Expression levels were calculated using the $2\Delta\Delta^{-Ct}$ method.

PCR amplification, cloning and sequencing of PCR products

Sorted total naive, $CD27^{dull}$ and $CD27^{bright}$ MBC subsets were amplified by PCR. We separately amplified IgM and IgG sequences using isotype-specific universal reverse primers CH1-Cμ and CH1-Cγ (Aranburu et al., 2010). Ig VH families were amplified using specific forward primers for each family: L-VH1; L-VH3; L-VH4/6 and L-VH5. We ran 30 PCR cycles/sample using the Titan One Tube RT-PCR System (Roche). The PCR error was calculated according to Aranburu et al., (2010) (*61)*. We sequenced beta-actin clones from sorted cells and established the PCR error frequency as 0.036%. $CD27^{-}$ naive B cells sorted from PB had a mutation frequency of 0.025%, a value similar to the PCR error frequency. PCR products were separated on agarose gel, purified using Wizard SV Gel and PCR Clean-Up System (Promega) and subcloned using the Zero Blunt TOPO PCR cloning kit (LifeTechnologies). Plasmid DNA was purified using the 96-well plate format of the MACHEREY-NAGEL NucleoSpin® 8/96 Plasmid Kit (GmbH & Co. KG), according to the instructions supplied by the manufacturers and inserts were sequenced in our laboratory using an ABI3730 DNA analyzer (LifeTechnologies) with the BigDye Terminator v3.1 Cycle Sequencing kit (LifeTechnologies). Per-base accuracy of Sanger sequencing is 99.999%.

Mutation and VH gene segment analysis

Germline sequences were aligned with the obtained sequences using the V-QUEST tool provided by the international ImMunoGeneTics (IMGT) information system (http://www.imgt.org). Because of the partial overlap with forward primer sequences we exclude the first nine nucleotides of each VH region from the analysis. Mutation frequency values (%) were calculated by dividing the absolute number of nucleotide substitutions by the number of nucleotides from FR1 to the end of FR3, defined according to IMGT's unique numbering, and multiplied by 100 (Aranburu et al., 2017). Ratios of replacement (R) or silent (S) mutations are defined as number of mutations/total number of sequenced clones. Mutation range was calculated by classifying every sequenced clone into one of four groups: 0, 1-to-3, 4-to-10 or > 10 mutations. Unproductive and duplicate clones were discarded from the analysis.

QUANTIFICATION AND STATISTICAL ANALYSIS

All sample sizes can be found in figure legends. Depending on if the datasets were normally distributed either Mann-Whitney non-parametric test or unpaired Student's t test were used. The Chi-square test with 5x5 (or less) contingency tables was used to compare mutation range values. A level of $p < 0.05$ was considered statistically significant. Basic characteristics of IG repertoires, somatic mutation frequencies between $CD27^{dull}$ and $CD27^{bright}$ subsets, and replacement-to-silent mutations ratio between $CD27^{dull}$ and $CD27^{bright}$ subsets were compared using the Tukey's honest significant difference test. Proportion of each isotype usage between pairs of subsets was compared using two-tailed Student's t test with Benjamini-Hochberg correction. Proportions of all isotypes usage across three subsets, as well as proportions of all isotypes usage between $CD27^{dull}$ and $CD27^{bright}$ subsets was compared using two way Anova, log(proportion of isotype).

DATA AND CODE AVAILABILITY

This study used computer codes and algorithms that are available in the documentation for each of the softwares (MIGEC, MIXCR and VDJ tools; see Key Resources Table for links). Original/source data for figures in the paper is available upon request.

The data that support the findings of this study are openly available in figshare at https://doi.org/10.6084/m9.figshare.11592036 and https://doi.org/10.6084/m9.figshare.11592027. RNA-seq data are available in NCBI-SRA, and the reference number of the paper is SRP241753.